Non-conservative circular dichroism of photosystem II reaction centers: Is there an enhancement by a coupling with charge transfer states?

Dominik Lindorfer[1*], Frank Müh[1], Robin Purchase[2*], Elmars Krausz[2], Thomas Renger[1]

1. Institute for Theoretical Physics
   Johannes Kepler University, Linz
   Altenbergerstrasse 69, 4040 Linz, Austria.
2. Research School of Chemistry
   Australian National University
   Canberra, ACT 2601, Australia

* Corresponding authors: robin.purchase@anu.edu.au, Dominik.Lindorfer@jku.at

Abstract

The non-conservative nature of the circular dichroism (CD) spectrum of the Q_y spectral region of the D1/D2/Cytb_{559} reaction center complexes of photosystem II is investigated. Our theory, in addition to the usual excitonic couplings between the Q_y transitions of the chlorophyll and pheophytin pigments, takes into account the coupling of the Q_y with the higher-energy B_x, B_y and N_{x+xy} transitions of these pigments and with $S_0 \rightarrow S_2$ transitions of the two β-carotene pigments close to the reaction center. The higher-energy transitions are parameterized by quantum chemical calculations and an analysis of the experimental oscillator strength of the isolated pigments. The excitonic couplings between pigments are obtained with the Poisson-TrEsp method. The coupling between exciton and charge transfer states in the central P_{D1}-P_{D2} dimer is implicitly taken into account by a scaling factor of the excitonic coupling. The observed non-conservativity of the Q_y CD spectrum can be qualitatively understood by the above described mixing of Q_y and higher-energy transitions. The analysis suggests that the non-conservativity may be enhanced by coupling to charge transfer states. We expect that the present study will stimulate explicit microscopic studies of the charge transfer states in the reaction center of photosystem II.

Keywords

Pigment-protein complexes, optical spectra, Frenkel exciton Hamiltonian, site energies, excitonic couplings

Abbreviations

PSII – Photosystem II
RC – Reaction center
CD – Circular dichroism
Chl – Chlorophyll
Car – Carotenoid
PPC – Pigment-protein complex
CT – Charge transfer
PDA – Point-dipole approximation
Pheo – Pheophytin
SI – Supplementary information
XC – Exchange correlation
DFT – Density functional theory

1. Introduction

A very attractive feature of circular dichroism (CD) spectra of molecular aggregates in general and photosynthetic pigment-protein complexes (PPCs) in particular is that these spectra are often dominated by the chirality of the exciton wavefunction rather than by the chirality of the pigments themselves. The planar chlorin pigments of photosynthesis in general have a very small intrinsic rotational strength; but, because of the partial delocalization of the excited states over different pigments, the exciton states gain the significant rotational strength that is displayed in the CD spectrum. This feature makes the CD spectrum particularly sensitive to the relative orientations and distances between chromophores within a PPC.

The PPC structure determines the mutual orientation of the transition dipole moments of the pigments entering the rotational strength of exciton states explicitly (see below), whereas the molecular structure determines the local excitation energies of the pigments, termed site energies [1]. These factors combine to influence the delocalization of the exciton states and thereby their rotational strength. Therefore, CD spectra provide valuable data for the evaluation of exciton Hamiltonians of PPCs [2].

If two optical transitions on different pigments occur at very different energies, their quantum mechanical mixing, and hence the influence of their coupling on the CD spectra, will be small. For this reason, to a good approximation, the low energy region of the CD spectrum of PPCs can often be described well by considering the Q_y transitions of the chlorin pigments and their mutual couplings alone. A good check of the limitations of such a description is to take the integral over the low energy region of the CD spectrum. If this integral is zero, the spectrum is termed conservative and it can be assumed that neither the intrinsic CD of the pigments nor the excitonic coupling between Q_y and high-energy transitions has a contribution in the low energy region.

There are, however, cases where the regions of positive and negative CD are not equal, and the spectrum becomes non-conservative. We have recently presented an extension of the standard model and explained the strongly negative integral over the Q_y CD spectrum of the CP29 complex of higher plants, by taking into account the coupling between Q_y and high-energy transitions of the pigments [3]. Another example of a complex with a strongly non-conservative low-energy CD spectrum is the D1/D2/Cytb_{559} reaction center complex of photosystem II of higher plants [4, 5], shown in Fig. 1.

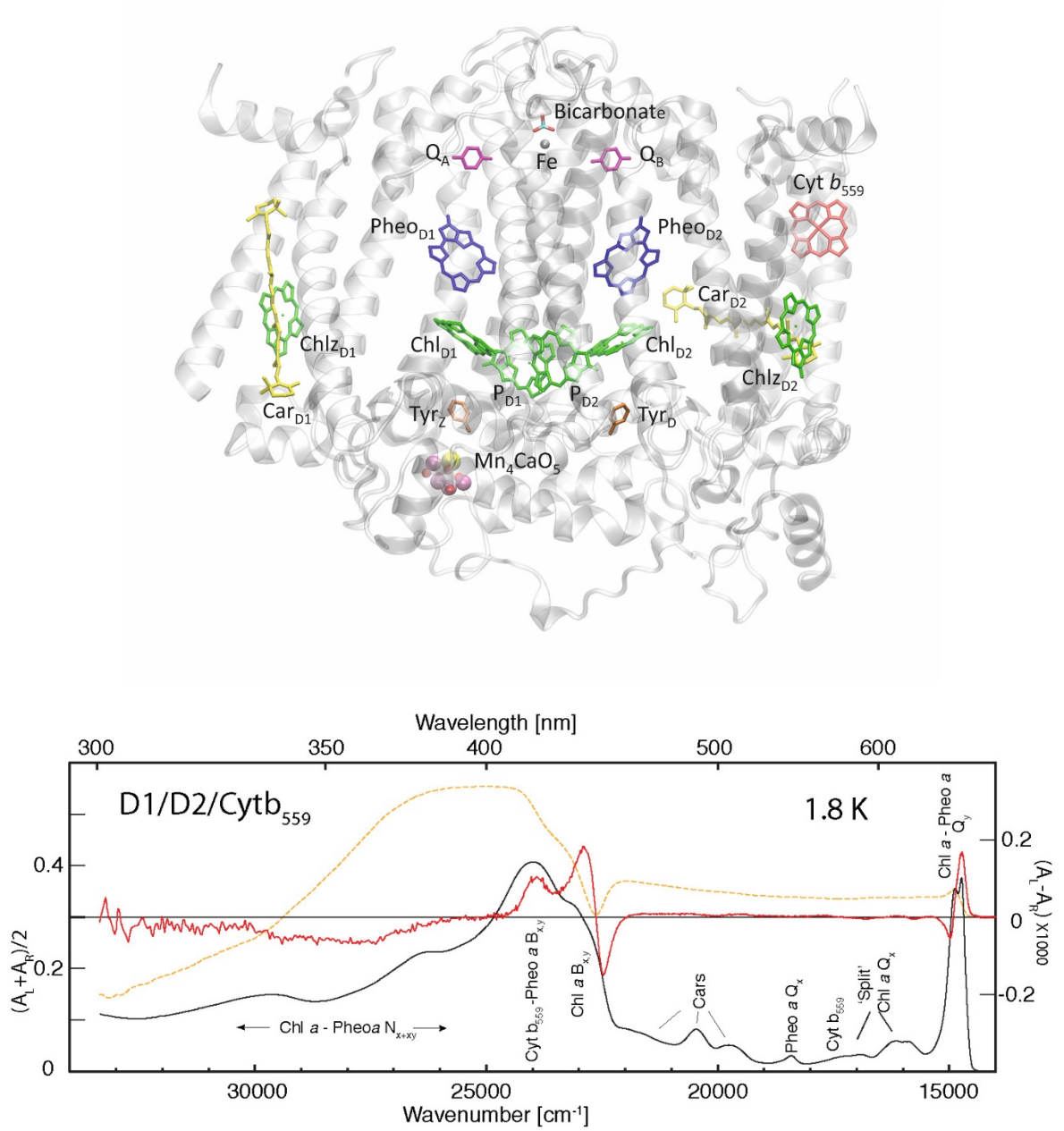

Fig. 1: ***Upper part****: Structure of the D1/D2/Cytb$_{559}$ complex based on the data by Kern et al. [5] and visualized using VMD [6]. The protein backbone corresponds to D1, D2, Cytb$_{559}$, and PsbI. Chl a pigments are shown in green, Pheo a pigments in blue, β-carotene in yellow, and the Cytb$_{559}$ heme in red. Also shown are the redox-active tyrosines Tyr$_Z$ and Tyr$_D$ as well as the Mn$_4$CaO$_5$ cluster and the quinones Q_A and Q_B (surrounding the none-heme iron Fe with bound bicarbonate), which are missing or inactive compared with the same redox component in an intact PSII core complex.* ***Lower part****: Low temperature (1.8 K) absorption (black solid line, left-hand scale) and CD (red solid line, right-hand scale) with its accompanying integral (yellow dashed line) of the PSII reaction center showing not only the low-energy Q bands, but also the high-energy B and N bands.*

The reaction center contains two quasi-symmetric branches (D1 and D2) of cofactors that determine the optical spectra in the visible spectral region and the electron transfer properties

[7]. The low temperature (1.8 K) linear absorption and CD spectra of this complex in the UV/VIS spectral region are shown in the lower part of Fig. 1. The low-energy band around 650 nm is due to the Q_y transitions of the chlorines (Chls and Pheos) and the second major band around 430 nm is termed the Soret band. Between these two bands, some minor additional bands appear in the absorption spectrum, e.g., due to the Q_x transitions of the chlorine pigments. In the CD spectrum these minor bands are suppressed because of the low intrinsic CD of the underlying transitions and their small excitonic couplings resulting from the small oscillator strength. The focus of the present work is on the analysis of the Q_y region of the CD spectrum. It exhibits a strongly positive integral, see Fig. 2, that requires explanation.

The Q_y exciton Hamiltonian of this complex is well understood from fitting of experimental spectra [8-11] and from independent quantum chemical/electrostatic calculations [12]. In this asymmetric exciton model the pigments in the two quasi-symmetric D1 and D2 branches, except for the central P_{D1} / P_{D2} dimer pigments, have different site energies. The chlorophyll Chl_{D1} in the D1-branch is the pigment with the lowest site energy and the pheophytin of the D2-branch, $Pheo_{D2}$, has the second lowest site energy.

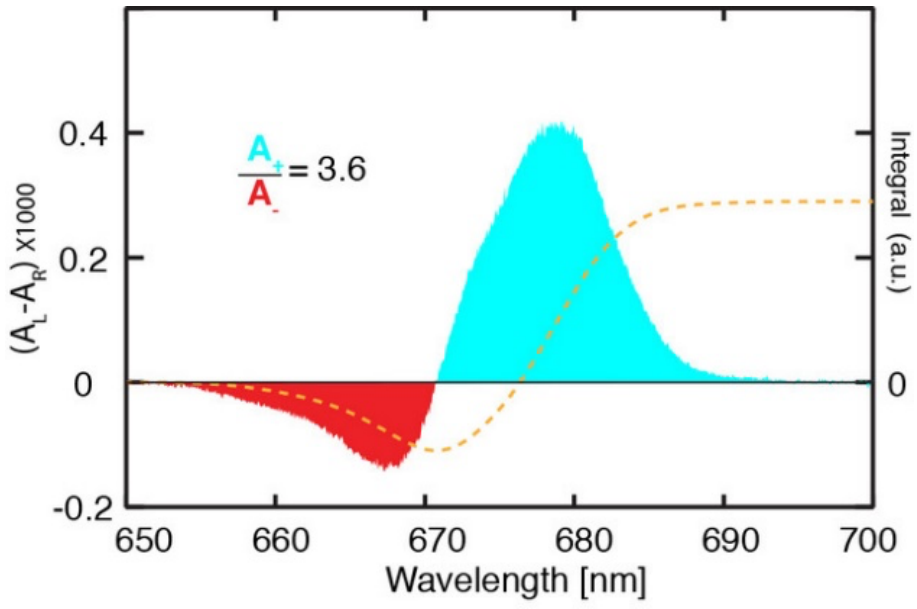

Fig. 2: Enlarged view on the experimental CD spectrum (left-hand scale) of D1/D2/Cytb$_{559}$ in the Q_y spectral region [13]. The strongly non-conservative nature is displayed by the ratios of positive (blue) to negative (red) areas. The integral of the CD is shown with a yellow dashed line (right-hand scale).

A key point that needs to be better understood is how the optical spectra of this complex are influenced by the coupling between exciton and charge transfer (CT) states.

In functionally intact PSII core complexes derived from higher plants, cyanobacteria and red algae, a broad 'red tail' extending out to 730 nm has been observed. This spectral feature is homogeneously broadened [14-17]. It has been suggested that the close proximity of P_{D1} and P_{D2} may enable electronic overlap between these pigments to the extent that a CT state borrows oscillator strength from the excited states and becomes weakly optically allowed. Stark spectra of D1/D2/Cytb$_{559}$ complexes helped Novoderezhkin et al. [10] to include a P_{D1}-P_{D2} CT state close in energy to the lowest exciton state. This state was proposed to exhibit a strong inhomogeneous broadening. It was coupled by ~35 cm^{-1} interaction to the excited states of the P_{D1}-P_{D2} special pair. The authors of this paper stated that this CT state is consistent with the 'red tail' observed in PSII core complexes. However, experimental observations [18] show that (1) no equivalent 'red tail' is observed in experiments on isolated D1/D2/Cyt*b*$_{559}$ complexes and (2) the low energy 'red tail' band observed on PSII core complexes is homogeneously rather than inhomogeneously broadened. Gelzinis et al. [11] reanalyzed the Stark spectra, using a different lineshape theory, and came to the conclusion that the low energy band in the Stark spectrum is influenced by the Chl_{D1}^{+}-$Pheo_{D1}^{-}$ CT state, which is red-shifted by ~ 500 cm^{-1} with respect to the lowest exciton state and coupled to the localized excited states of Chl_{D1} and $Pheo_{D1}$ by a 125 cm^{-1}-magnitude interaction.

A related and open question concerns the strength of the excitonic coupling between the Q_y transitions of P_{D1} and P_{D2}. Because of the small intermolecular distance, the point-dipole approximation (PDA) becomes invalid [19] and short-range contributions, which are due to wavefunction overlap giving rise to electron exchange, have to be taken into account [20]. Error compensation in the PDA modelling leads to excitonic coupling parameters that give reasonable agreement with experimental data [10]. From quantum chemical calculations on the entire P_{D1}-P_{D2} dimer and the same pigments as isolated monomers, a short-range contribution of 70 to 140 cm^{-1} to the excitonic coupling in the special pair has been determined [20]. This estimate takes into account a superexchange type mixing with a high-energy CT state. Including long-range and short-range excitonic coupling processes in the fit of optical spectra revealed an optimal range of the interaction parameter between 140 and 170 cm^{-1} [9]. In the present work we will use a value of 160 cm^{-1} for this coupling, which is roughly twice the long-range contribution, that is due to the Coulomb interaction between

transition densities, obtained with the Poisson-TrEsp method. We also consider a related enhancement of the P_{D1}-P_{D2} excitonic couplings involving higher-energy transitions.

An important component of this work is that computationally derived absorption and CD spectra are compared to experimental data, for which CD and absorption have been measured simultaneously. This approach avoids ambiguities and errors related to sample variability, resolution and calibration differences, which are inherent when CD and absorption are measured on different instruments. By means of simultaneous measurement, absorption and CD spectra can confidently be compared absolutely. This leads to an extra check of our model: as well as the calculated spectral profiles in absorption and CD being compared to data, the relative amplitude of the CD to absorption can also be compared.

In this work we first provide a summary of our earlier theory [3] on non-conservative CD spectra and discuss the parametrization of the extended exciton Hamiltonian by quantum chemical/electrostatic calculations and an analysis of optical spectra of the isolated pigments. Next, the theory is applied to calculate low temperature (1.8 K) CD and absorption spectra of D1/D2/Cytb_{559} complexes and the results are compared with experimental data. We provide an explanation of the non-conservative nature of the Q_y CD spectrum and consider the role of CT states implicitly by rescaling the intra special pair excitonic couplings.

2. Experimental methods

The single spectrometer system used here [21] has the advantage that simultaneous and/or parallel spectroscopic measurements can be made on a single biochemical sample. Photosynthetic protein preparations can be both variable and fragile. Being able to measure the same sample in the same spectrometer system, without having to thermally cycle or otherwise change the sample is a significant advantage. Spectra collected in this manner are directly comparable to each other. Furthermore, protocols, procedures, and sample handling systems have been developed to prevent the sample from being degraded by exposure to light, air or ambient temperatures.

The properties and biochemical preparation of D1/D2/Cytb_{559} samples sourced from spinach have been described in detail [22]. The samples used for optical experiments were diluted to 55% with a 1:1 glycerol/ethylene glycol mixture (v/v) as glassing agent. Specialized strain-free, cylindrical fused-quartz sample cells of 12 mm diameter and 0.2 mm to 1mm in pathlength were used. These cells have also been described [23].

3. Theory

The Hamiltonian of the pigment-protein complex contains three contributions

$$H = H_{\mathrm{ex}} + H_{\mathrm{ex-vib}} + H_{\mathrm{vib}} \tag{1}$$

The electronic degrees of freedom of the pigments are contained in the excitonic Hamiltonian H_{ex}, the coupling between the electronic and the nuclear degrees of freedom is described by the exciton-vibrational Hamiltonian $H_{\mathrm{ex-vib}}$, and the dynamics of nuclear degrees of freedom is given by H_{vib}. Explicit expressions for H_{vib} and $H_{\mathrm{ex-vib}}$ are given in refs [24] and [3]. The excitonic Hamiltonian is split into three contributions

$$H_{\mathrm{ex}} = H_{\mathrm{ex}}^{(\mathrm{Q}_y)} + H_{\mathrm{ex}}^{(\mathrm{he})} + V_{\mathrm{Q}_y,\mathrm{he}} \tag{2}$$

where $H_{\mathrm{ex}}^{(\mathrm{Q}_y)}$ contains the Q_y transitions of the 6 chlorophyll *a* (Chl *a*) and 2 Pheophytin *a* (Pheo *a*) pigments of the D1/D2/Cytb_{559} complex, which are characterized by their local transition energies $E_m^{(\mathrm{Q}_y)}$ and excitonic couplings $V_{mn}^{(\mathrm{Q}_y)}$:

$$H_{\mathrm{ex}}^{(\mathrm{Q}_y)} = \sum_m E_m^{(\mathrm{Q}_y)} |m\rangle\langle m| + \sum_{m,n}^{m\neq n} V_{mn}^{(\mathrm{Q}_y)} |m\rangle\langle n| \tag{3}$$

Here, $|m\rangle$ denotes an electronic excited state of the complex, in which pigment *m* is in its first excited state (S_1) and all other pigments are in their electronic ground state (S_0).

The eigenstates of the Q_y exciton Hamiltonian $H_{\mathrm{ex}}^{(\mathrm{Q}_y)}$ are given as $|M^{(0)}\rangle = \sum_m c_m^{(M)} |m\rangle$. The Hamiltonian of the high-energy states $H_{\mathrm{ex}}^{(\mathrm{he})}$ of the reaction center pigments, which include two β-carotene (Car) molecules besides the Chl *a* and Pheo *a* pigments, reads

$$H_{\mathrm{ex}}^{(\mathrm{he})} = \sum_{k,a} E_k^{(a)} |ka\rangle\langle ka| + \sum_{k,l}^{k\neq l} \sum_{a,b} V_{ka,lb}^{(\mathrm{he})} |ka\rangle\langle lb| \tag{4}$$

where *k* counts the pigments and *a* counts the high-energy excited states. In the case of the Chls and Pheos, we take into account the B_x, B_y and N_{x+xy} states, and for the Cars, the S_2 state, which will be characterized by quantum chemical calculations and experimental data below. The eigenstates of $H_{\mathrm{ex}}^{(\mathrm{he})}$ are given as $|\widetilde{M}\rangle = \sum_{k,a} c_{ka}^{(\widetilde{M})} |ka\rangle$. The last term in Eq. 2 contains the couplings between the Q_y transition and the high-energy transitions of different pigments

$$V_{\mathrm{Q}_y,\mathrm{he}} = \sum_m \sum_{a,b} V_{m,ka}^{(\mathrm{Q}_y,\mathrm{he})} |m\rangle\langle ka| + \mathrm{h.\,c.} \tag{5}$$

$V_{m,ka}^{(\mathrm{Q}_y,\mathrm{he})}$ is the excitonic coupling between the Q_y transition of pigment *m* and the excitation of the *a*th excited state of pigment *k*.

We use first-order perturbation theory to treat the couplings in Eq. 5 and obtain the following mixing between the eigenstates of the bare Q_y exciton Hamiltonian (Eq. 3) and the eigenstates of the high energy exciton Hamiltonian (Eq. 4): $|M\rangle \approx \left|M^{(0)}\right\rangle + \sum_{\widetilde{M}} \eta(N,\widetilde{M})\left|\widetilde{M}\right\rangle$, with the mixing coefficient

$$\eta\left(N,\widetilde{M}\right) = \frac{V_{M,\widetilde{M}}}{E_M - E_{\widetilde{M}}} \tag{6}$$

Here, $V_{M,\widetilde{M}} = \sum_{m,k,a} c_m^{(M)} c_{ka}^{(\widetilde{M})} V_{m,ka}^{(\mathrm{Q}_y,\mathrm{he})}$ describes the coupling between exciton states $\left|M^{(0)}\right\rangle$ of the Q_y and $\left|\widetilde{M}\right\rangle$ of the high-energy state manifold, $V_{m,ka}^{(\mathrm{Q}_y,\mathrm{he})}$ is the coupling between the local excited states $|m\rangle$ and $|ka\rangle$ in Eq. 5, and $c_m^{(M)}$ and $c_{ka}^{(\widetilde{M})}$ are the coefficients of the eigenstates of $\left|M^{(0)}\right\rangle$ and $\left|\widetilde{M}\right\rangle$, respectively. The use of first-order perturbation theory is justified by the fact that $\eta\left(N,\widetilde{M}\right) \ll 1$. The numerical values of the excitonic couplings $V_{m,ka}^{(\mathrm{Q}_y,\mathrm{he})}$ are given in a supplementary data file. Because of these couplings, the Q_y electric and magnetic transition dipole moments are modified. Taking into account these modifications and neglecting the intrinsic magnetic transition dipole moments of the pigments, the following expression for the CD spectrum ensues [3]

$$CD(\omega) = \frac{8\pi^3 n_{\mathrm{mol}}\omega}{3\hbar c n_{\mathrm{r}} \lambda_0} \sum_M D_M(\omega) \left(\sum_{m,n}^{m>n} c_m^{(M)} c_n^{(M)} \left(\vec{R}_m - \vec{R}_n\right) \cdot \left(\vec{\mu}_m \times \vec{\mu}_n\right) \right.$$

$$\left. + \frac{\lambda_0}{\bar{\lambda}} \sum_{\widetilde{M}} \eta\left(M,\widetilde{M}\right) \sum_{m,k,a} c_m^{(M)} c_{ka}^{(\widetilde{M})} \left(\vec{R}_m - \vec{R}_k\right) \cdot \left(\vec{\mu}_m \times \vec{\mu}_{ka}\right) \right) \tag{7}$$

where n_{mol}, n_{r} and c are the molecular density, the refractive index of the sample and the velocity of light in vacuum, respectively. The CD calculated using Eqn. 7 becomes zero in the absence of excitonic couplings.

The lineshape function $D_M(\omega)$ takes into account exciton-relaxation-induced lifetime broadening and excitation of vibrational sidebands, as described in refs [24] and [3]. The coefficients $c_m^{(M)}$ of the Q_y exciton states and the $c_{ka}^{(\widetilde{M})}$ of the high-energy exciton states are obtained from the diagonalization of the respective exciton Hamiltonians (Eqs. 3 and 4) and $\vec{R}_l$ denotes the center of pigment *l*. The center of each Chl *a* and Pheo *a* is taken as the midpoint of the line connecting their $\mathrm{N_B}$ and $\mathrm{N_D}$ atoms, while the center of the Cars is

defined as the center of the C7-C27 axis of the polyene chain. The Q_y transition dipole moment $\vec{\mu}_l$ of pigment l is assumed to be oriented along the y-axis, defined by the $\mathrm{N_B} - \mathrm{N_D}$-direction, and the magnitude is estimated from experiment as described below. The transition dipole moment $\vec{\mu}_{ka}$ of the excitation of the ath high energy state of pigment k is obtained from quantum chemical calculations and experimental data, as will be described below. Finally, the wavelengths λ_0 and $\bar{\lambda}$ are average wavelengths of the Q_y and of all the relevant transitions, respectively, of the pigments. The ratio $\lambda_0/\bar{\lambda}$ is approximately 1.5 using a λ_0 in the 670 nm range, and a $\bar{\lambda}$, which is dominated by the high-energy transitions, of about 450 nm.

The first term in Eq. 7 contains the conservative part of the CD spectrum and the second line contains the influence of higher excited states that leads to a non-zero integral I over the Q_y spectral region of the CD spectrum

$$I = \int_{\mathrm{Q}_y} d\omega \frac{CD(\omega)}{\omega}$$

$$= \frac{8\pi^3 n_{\mathrm{mol}}}{3\hbar c n_{\mathrm{r}} \bar{\lambda}} \sum_M \sum_{\widetilde{M}} \eta\left(M, \widetilde{M}\right) \sum_{m,k,a} c_m^{(M)} c_{ka}^{(\widetilde{M})} \left(\vec{R}_m - \vec{R}_k\right) \cdot \left(\vec{\mu}_m \times \vec{\mu}_{ka}\right) \quad (8)$$

To see more clearly which factors lead to a non-conservative CD spectrum, we approximate the mixing coefficient in Eq. 6 as

$$\eta\left(N, \widetilde{M}\right) = \frac{V_{M,\widetilde{M}}}{E_M - E_{\widetilde{M}}} \approx -\frac{V_{M,\widetilde{M}}}{\Delta E} = -\sum_n \sum_{l,b} c_n^{(M)} c_{lb}^{(\widetilde{M})} V_{n,lb}^{(\mathrm{Q}_y,\mathrm{he})} / \Delta E \quad (9)$$

where ΔE is an average energy gap between the high energy and the Q_y transitions. By introducing this approximate $\eta\left(N, \widetilde{M}\right)$ in Eq. 8, and taking into account that $\sum_M c_m^{(M)} c_n^{(M)} = \delta_{m,n}$ and $\sum_{\widetilde{M}} c_{ka}^{(\widetilde{M})} c_{lb}^{(\widetilde{M})} = \delta_{k,l}\delta_{a,b}$, the integral becomes

$$I \approx -\frac{8\pi^3 n_{\mathrm{mol}}}{3\hbar c n_{\mathrm{r}} \bar{\lambda} \Delta E} \sum_{m,k,a} V_{m,ka}^{(\mathrm{Q}_y,\mathrm{he})} \left(\vec{R}_m - \vec{R}_k\right) \cdot \left(\vec{\mu}_m \times \vec{\mu}_{ka}\right) \quad (10)$$

It is thus seen that the non-conservativity of the CD spectrum depends neither on the excitonic Hamiltonian of the $\mathrm{Q_y}$ transitions, nor on that of the higher-energy transitions but rather on the coupling between them and on the relative orientation and magnitudes of the transition dipole moments of these transitions. Note, that the approximation in Eq. 9 is only used for the interpretation of the results, which are obtained using the original expression for $\eta\left(N, \widetilde{M}\right)$ (Eq. 6).

Along the same lines as for the CD spectrum, the linear absorption spectrum is [3]

$$\alpha(\omega) = \frac{4\pi^2 n_{\mathrm{mol}}\omega}{3\hbar c n_{\mathrm{r}}} \sum_M D_M(\omega) \left(\left| \mu_M^{(0)} \right|^2 + 2 \sum_{\widetilde{M}} \eta\left(N, \widetilde{M}\right) \vec{\mu}_M^{(0)} \cdot \vec{\mu}_{\widetilde{M}} \right) \tag{11}$$

where $\vec{\mu}_M^{(0)} = \sum_m c_m^{(M)} \vec{\mu}_m^{(\mathrm{Q}_y)}$ is the transition dipole moment of the Mth eigenstate of the bare Q_y exciton Hamiltonian (Eq. 3) and similarly $\vec{\mu}_{\widetilde{M}} = \sum_{k,a} c_{ka}^{(\widetilde{M})} \vec{\mu}_{ka}^{(\mathrm{he})}$ is that of the $\widetilde{M}$th eigenstate of the high energy exciton Hamiltonian (Eq. 4).

4. Computational Methods and Parameterization of Hamiltonian

The local Q_y transition energies $E_m^{(\mathrm{Q}_y)}$ of the pigments were taken from earlier work [12], having been obtained from quantum chemical/electrostatic calculations and a fit of optical spectra, albeit with one alteration: all site energies are blue-shifted by 1.5 nm, an adjustment that leads to an improved fit of the present low-temperature optical spectra. The site energies are given in Table S5 of the Supplementary Information (SI). Since in the present study the influence of the higher excited states on the non-conservativity of the CD spectrum in the Q_y spectral region is of main interest, the exact values of the excitation energies $E_k^{(a)}$ are not needed. It is important to keep in mind that the integral over the CD spectrum in Eq. 10 only depends indirectly and weakly on the $E_k^{(a)}$, via the average energy ΔE (Eq. 9). For simplicity, we assume the same $hc/E_k^{(\mathrm{Chl}a,\mathrm{B}_x)} = 420$ nm, $hc/E_k^{(\mathrm{Chl}a,\mathrm{B}_y)} = 420$ nm, and $hc/E_k^{(\mathrm{Chl}a,\mathrm{N}_{x+xy})} = 400$ nm for the B_x, B_y and N_{x+xy} transitions respectively, for all Chl *a* pigments. The corresponding wavelengths for the two Pheo *a* pigments are $E_k^{(\mathrm{Pheo},\mathrm{B}_x)} = 415$ nm, $hc/E_k^{(\mathrm{Pheo},\mathrm{B}_y)} = 415$ nm, and $E_k^{(\mathrm{Pheo},\mathrm{N}_{x+xy})} = 400$ nm. Finally, the $\mathrm{S}_0 \rightarrow \mathrm{S}_2$ transition wavelength is given as $hc/E_k^{(\mathrm{Car})} = 490$ nm. An estimate of these energies was obtained from spectra of the isolated pigments in solution, which were also used to calibrate the dipole strengths of these transitions, as will be discussed below and in the SI. The exact values of the excitation energies of these high-energy transitions have practically no influence on the spectra in the Q_y spectral region (Fig. S7).

The excitonic couplings $V_{mn}^{(\mathrm{Q}_y)}$ and $V_{ka,lb}^{(\mathrm{he})}$ between the Q_y transitions and between the high-energy transitions, respectively, is obtained with the Poisson-TrEsp method [25, 26]. In this method, atomic transition charges are determined from a least-mean square fit of the

electrostatic potential (ESP) of the transition density obtained with quantum chemical calculations on the isolated pigments. These transition charges are rescaled to yield the correct vacuum transition dipole moment that can be estimated from the oscillator strength of the relevant pigment transition in different solvents [27]. In this way, a vacuum transition dipole of 4.58 D was obtained for the Q_y transition of Chl *a* [27]. The vacuum dipole strengths of the remaining transitions of Chl *a* and of the transitions of the other pigments are obtained from their relative dipole strength with respect to Chl *a* in a given solvent and assuming that the same ratio applies to the vacuum dipole strengths. More details on this estimate can be found in ref [3] and in the SI. The vacuum transition charges are placed into molecule-shaped cavities representing the pigments with optical dielectric constant 1 inside and 2 outside the cavities. A Poisson equation is solved for the ESP of the transition density, and from that ESP of one pigment, and the transition charges of the other, the coupling between transition densities of the two different pigments in the dielectric environment is obtained. The geometry optimization of the isolated pigments was done with density functional theory (DFT) using the B3LYP exchange correlation (XC) functional and a 6-31G** basis set.

The calculation of the transition densities was performed with time-dependent DFT and different XC-functionals (B3LYP, BHHLYP, the long-range corrected CAM-B3LYP) within the random phase approximation, and also with the wavefunction-based HF/CIS method, using a 6-31G* basis set in all excited state calculations. All computations have been carried out using the program Q-Chem [28] and using the crystal structure of the RC of PSII based on PDB 3WU2 at 1.9 Å [4]. The excitonic couplings between Q_y transitions obtained in this way are given in SI Table 4. The couplings between the Q_y and the high energy transitions, as well as the couplings between the high-energy transitions themselves are available in a data file in the SI.

Because of the wavefunction overlap between the special pair pigments P_{D1} and P_{D2}, their excitonic coupling contains a significant contribution from short-range interactions. A value of 140-170 cm^{-1} has been estimated previously [9] from a fit of several linear optical spectra. A value of 160 cm^{-1} is used here instead of the purely Coulombic part, for which, with the Poisson-TrEsp method, we obtain a value that varies between 72 cm^{-1} from TDDFT with the B3LYP XC-functional, and 95 cm^{-1} obtained with HF-CIS. Please note also, that a short-range contribution of 70 – 140 cm^{-1} has been estimated from quantum chemical calculations [20] as mentioned above. Similar effects were reported for the special pairs of purple bacteria

and photosystem I [29]. As discussed above, there is a ~2x enhancement of the excitonic coupling between the Q_y transitions of P_{D1} and P_{D2} caused by the coupling to charge transfer states. It is very likely that the excitonic couplings involving higher-energy transitions of the special pair are also affected by coupling to intermolecular charge transfer states. For simplicity, we assume that all the couplings between P_{D1} and P_{D2} are enhanced by the same factor *x*. We further study the effect of this enhancement factor on the non-conservativity of the CD spectrum.

The electrostatic potentials of the Q_y, B_x, B_y and the N_{x+xy} transition densities of Pheo *a*, and the $S_0 \rightarrow S_2$ transition of β-carotene are shown in Figs. S3 and S4. In both Pheo *a* and Chl *a*, two strong and nearly orthogonal higher-energy transitions (B_x, B_y) as well as a transition with mixed xy polarization (N_{x+xy}) are found. Other transitions are expected to only make small contributions to the optical spectra discussed below, either because of their small dipole strength (e.g. Q_x) or because they are further off-resonant with respect to the Q_y transition than the Soret transitions. The transition charges for all transitions included in our analysis are rescaled to yield the dipole strength obtained from the experimental absorption spectra on the isolated pigment measured in 80% acetone, as described above, and the resulting vacuum transition dipole strengths for the transitions of Pheo *a* and the β-carotene $S_0 \rightarrow S_2$ transition are given in SI Tables S2 and S3, respectively. For simplicity, the Q_y and B_y transition dipole moments are oriented approximately along the y-axis of Chl *a* and Pheo *a*, which is defined by their N_B-N_D atoms (in PDB nomenclature) and that of the B_x transition along the *x*-axis, which is defined by the N_A-N_C atoms. The N_{x+xy} transition dipole moment is found to be rotated by approximately 30° with respect to the y-axis, and the β-carotene $S_0 \rightarrow S_2$ transition dipole moment is oriented along the polyene chain defined by the C7-C27 axis (in PDB nomenclature).

5. Results

The coupling between the Q_y and the high-energy transitions indeed leads to a non-conservative CD spectrum, as seen in Fig. 3 (lower panel). In particular, the strongly positive low-energy part of the experimental CD spectrum between 676 and 686 nm is well described by the calculations. Deviations between the calculations and experiment [13] remain between 672 and 676 nm, where the experimental spectrum is still positive and the calculations give a weak negative CD signal. The absorption spectrum (Fig. 3 upper panel) is less affected by the

higher-energy transitions than the CD spectrum. There is a slight broadening and a redistribution of oscillator strength from the central region (672-676 nm) towards the blue wing (662-668 nm). Both calculations (with and without the coupling to high-energy transitions) yield a somewhat too large oscillator strength of the low energy peak (around 678 nm) and a somewhat too small oscillator strength of the high energy peak/shoulder, as compared to the experimental data [13].

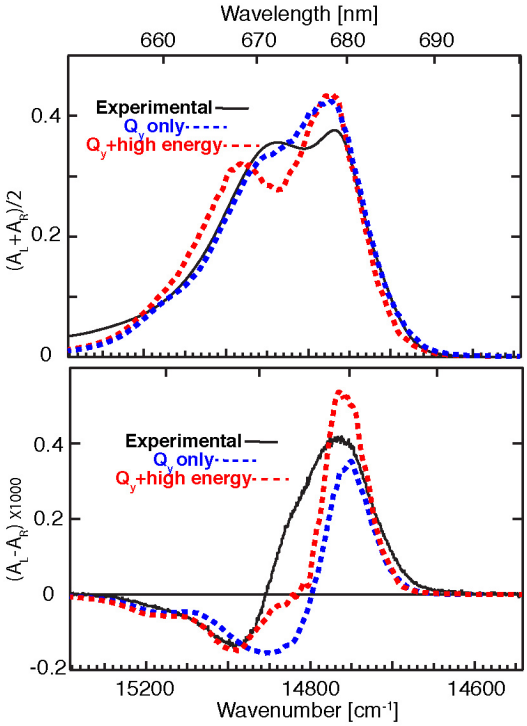

Fig. 3: Low-Temperature (1.8 K) absorption (upper) and CD (lower) spectra calculated with (red dashed line) or without (blue dotted line) the excitonic couplings between the Q_y transitions and the high-energy transitions of the pigments taken into account, compared to experimental data (solid black line [13].

To analyze the influence of the high-energy transitions on the non-conservativity of the CD spectrum, we use the ratio of areas above and below the zero line of the CD curve (A_+/A_- see Fig. 1) as a metric. Besides the coupling between Q_y transitions, we determined the coupling of the Q_y transitions to each particular type of higher-energy transition of the pigments (Fig. 4). There is no particular coupling dominating the non-conservativity of the CD spectrum; although the couplings to B_y and B_x transitions of the chlorins give a somewhat larger contribution than the couplings to N_{x+xy} transitions and to the $S_0 \rightarrow S_2$ transitions of the Cars. Whereas the smaller couplings are explained by the smaller dipole strength in the case of the N_{x+xy} transitions, it is the inter-pigment distance and orientation in

the case of the carotenoids. If all high-energy transitions are included, a ratio A_+/A_- = 2.6 is obtained for the CAM-B3LYP XC-functional, whereas the experimental value A_+/A_-= 3.6 is somewhat larger. Different quantum chemical methods give rise to very similar values of A_+/A_- (Fig. S6).

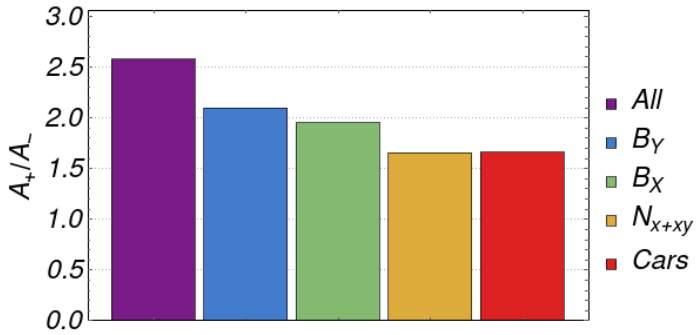

Fig. 4: Analysis of the influence of the coupling of Q_y to particular high-energy transitions B_x, B_y and N_{x+xy} on the non-conservativity of the CD spectrum, quantified by the ratio A_+/A_- as described in the text.

Additionally, we investigate how the non-conservativity of the Q_y CD spectrum depends on the enhancement of the excitonic couplings between P_{D1} and P_{D2} by coupling to CT states. Since the enhancement factor between the Q_y transitions of P_{D1} and P_{D2} has been estimated from a fit of optical spectra [9] and is supported also by independent quantum chemical calculations [20], we have not varied this factor, but considered different enhancement factors x for those intra special pair excitonic couplings that involve high-energy transitions. Here x = 1 corresponds to the long-range Coulombic part of the excitonic coupling. Interestingly, the non-conservativity A_+/A_- can be enhanced by the coupling to CT states (Fig. 5). It increases from A_+/A_-= 2.0 for x = 0.1 (corresponding to a suppression of the excitonic coupling by the CT states) to A_+/A_-= 2.9 for x = 3.

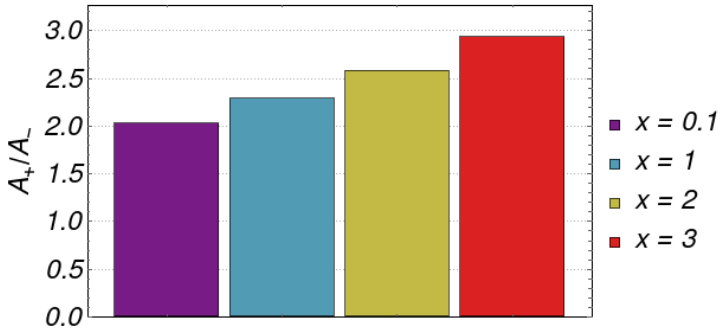

Fig. 5: Non-conservativity of the CD spectrum obtained using different enhancement factors x for the intra special pair excitonic couplings involving high-energy transitions. The corresponding CD spectra are shown in Figure S6.

As expected from Eq. 10, the CD spectra calculated for the Q_y spectral region are insensitive to the exact energies of the high-energy transitions, as demonstrated for the B-transitions in Fig. S7.

6. Discussion and Conclusions

The non-conservative nature of the low energy CD spectrum of D1/D2/Cytb_{559} complexes can be semi-quantitatively understood using the parameterized model presented. The model specifically takes into account the excitonic coupling between the Q_y states and the higher-energy transitions of the pigments. An important subtlety of the model concerns the way it introduces an effective treatment for coupling between exciton and charge transfer states. The process of fitting optical spectra [9] along with quantum chemical calculations [20] indicate a two-fold enhancement of the excitonic coupling between the Q_y transitions of P_{D1} and P_{D2} by short-range effects due to electron exchange between these two pigments. We propose an extension of the same enhancement to the excitonic coupling between the other local excitations in P_{D1}-P_{D2}. Although a crude approximation, it is perhaps the simplest possible choice, as it could be expected that the increased overlap of higher excited state wavefunctions leads to a larger enhancement of the excitonic coupling in higher excited states.

Assuming that excitonic couplings between P_{D1} and P_{D2} involving at least one high-energy transition are enhanced by a factor x = 3, the ratio A_+/A_- increases to 2.9 compared to the value of 2.6 obtained for x =2. The former ratio is closer to the experimental value of 3.6. A

quantitative description of the non-conservative spectrum most likely requires the explicit inclusion of charge transfer states in the exciton Hamiltonian.

Recently, methods were developed that enable the extraction of an effective Frenkel-charge-transfer Hamiltonian from quantum chemical calculations on molecular dimers [30]. Although these optically dark CT states have no direct influence on the CD spectrum (because of their vanishing transition dipole moments, see Eq. 10) they effectively change the excitonic couplings between the optically allowed transitions by mixing with them. This mixing can be very complex and the enhancement factor for every excitonic coupling can therefore be different. In fact, in extreme cases, the short-range contributions could compensate or overcompensate the long-range part of the excitonic coupling [31, 32]. In the case of overcompensation, the excitonic coupling would even switch sign.

Future work envisaged would be the investigation of how the individual CT coupling terms affect the relative intensities of optical absorptions. The present calculations suggest that there is a strong effect of the CT state coupling on the CD spectra. Exploring this effect in greater detail will help us to further refine the exciton Hamiltonian of PSII reaction centers. A better characterization of the charge transfer states will ultimately enable us to study the charge transfer processes in this system, as many mechanistic and kinetic details are still not well understood [7].

Another challenging problem is the calculation of the full UV/VIS CD spectrum associated with all Q, B and N transitions (Fig. 1, lower part). At present we have used approximate and averaged energies of high-energy transitions, since, in our perturbative model of the coupling between these transitions and the Q_y transitions, their exact energies do not matter (see Eq. 10 and Fig. S7). A first glance at the extended CD spectrum in Fig. 1, which includes contributions from both, B and N bands, suggests that the overall CD spectrum ultimately becomes conservative near 330 nm and hence additional electronic excitations might not have to be included to describe the UV/VIS spectrum by an exciton theory. On the other hand, there seems to be a systematic negative contribution to the CD spectrum from excited states at shorter wavelengths that need to be resolved and understood better. At present, we cannot exclude that ultimately also the optical excitations of the protein will have to be included in the model for a full understanding of the CD spectrum shown in Fig. 1.

It will be a challenge to extend the asymmetric Q_y exciton Hamiltonian of PSII reaction centers to include the higher-energy states of the pigments in more detail. This will require

the estimation of site energies for the higher excited states of each pigment in D2/D2/Cytb_{559} as well as their transition dipole characteristics. Quantum chemical calculations on isolated pigments, even those made using relatively high-level DFT and other methods, have been shown to give the wrong order of some of those transitions [33]. An alternative approach is to extract these values experimentally from an extrapolation of the transition energies of relevant pigments measured in different non-polar solvents and then parameterize the extended exciton Hamiltonian based on calculated site-specific shifts using our electrostatic methods, and a fit of the CD and absorption spectra of D1/D2/Cytb_{559} complexes over the entire spectral range from 300 to 720 nm, shown in Fig. 1.

7. References

1. Renger, T. and F. Muh, *Understanding photosynthetic light-harvesting: a bottom up theoretical approach.* Phys Chem Chem Phys, 2013. **15**(10): p. 3348-71.
2. Garab, G. and H. van Amerongen, *Linear dichroism and circular dichroism in photosynthesis research.* Photosynth Res, 2009. **101**(2-3): p. 135-46.
3. Lindorfer, D., F. Muh, and T. Renger, *Origin of non-conservative circular dichroism of the CP29 antenna complex of photosystem II.* Phys Chem Chem Phys, 2017. **19**(11): p. 7524-7536.
4. Umena, Y., et al., *Crystal structure of oxygen-evolving photosystem II at a resolution of 1.9 A.* Nature, 2011. **473**(7345): p. 55-60.
5. Kern, J., et al., *Structures of the intermediates of Kok's photosynthetic water oxidation clock.* Nature, 2018. **563**(7731): p. 421-425.
6. Humphrey, W., A. Dalke, and K. Schulten, *VMD: Visual molecular dynamics.* JOURNAL OF MOLECULAR GRAPHICS & MODELLING, 1996. **14**(1): p. 33-38.
7. Renger, T. and E. Schlodder, *Optical properties, excitation energy and primary charge transfer in photosystem II: theory meets experiment.* J Photochem Photobiol B, 2011. **104**(1-2): p. 126-41.
8. Raszewski, G., W. Saenger, and T. Renger, *Theory of optical spectra of photosystem II reaction centers: location of the triplet state and the identity of the primary electron donor.* Biophys J, 2005. **88**(2): p. 986-98.
9. Raszewski, G., et al., *Spectroscopic properties of reaction center pigments in photosystem II core complexes: revision of the multimer model.* Biophys J, 2008. **95**(1): p. 105-19.
10. Novoderezhkin, V.I., J.P. Dekker, and R. van Grondelle, *Mixing of exciton and charge-transfer states in Photosystem II reaction centers: modeling of Stark spectra with modified Redfield theory.* Biophys J, 2007. **93**(4): p. 1293-311.
11. Gelzinis, A., et al., *Spectroscopic properties of photosystem II reaction center revisited.* J Chem Phys, 2017. **147**(11): p. 115102.
12. Muh, F., M. Plockinger, and T. Renger, *Electrostatic Asymmetry in the Reaction Center of Photosystem II.* J Phys Chem Lett, 2017. **8**(4): p. 850-858.
13. Hall, J., et al., *New Perspectives on Photosystem II Reaction Centres.* Australian Journal of Chemistry, 2020.

14. Hughes, J.L., et al., *Charge separation in photosystem II core complexes induced by 690-730 nm excitation at 1.7 K.* Biochim Biophys Acta, 2006. **1757**(7): p. 841-51.
15. Hughes, J.L., et al. *What Is the Origin of the Highly Dispersive Quantum Efficiencies for Secondary Donor Oxidation at Low Temperature in Photosystem II*. 2008. Dordrecht: Springer Netherlands.
16. Krausz, E., et al., *Oxygen-evolving Photosystem II core complexes: a new paradigm based on the spectral identification of the charge-separating state, the primary acceptor and assignment of low-temperature fluorescence.* Photochemical & Photobiological Sciences, 2005. **4**(9): p. 744-753.
17. Langley, J., et al., *The deep red state of photosystem II in Cyanidioschyzon merolae.* Photosynthetica, 2018. **56**(1): p. 275-278.
18. Krausz, E., N. Cox, and S.P. Arskold, *Spectral characteristics of PS II reaction centres: as isolated preparations and when integral to PS II core complexes.* Photosynth Res, 2008. **98**(1-3): p. 207-17.
19. Madjet, M.E., A. Abdurahman, and T. Renger, *Intermolecular Coulomb Couplings from Ab Initio Electrostatic Potentials: Application to Optical Transitions of Strongly Coupled Pigments in Photosynthetic Antennae and Reaction Centers.* J. Phys. Chem. B, 2006. **110**: p. 17268-17281.
20. Renger, T., et al., *Structure-based modeling of energy transfer in photosynthesis.* Photosynth Res, 2013. **116**(2-3): p. 367-88.
21. Krausz, E., *Selective and differential optical spectroscopies in photosynthesis.* Photosynth Res, 2013. **116**(2-3): p. 411-26.
22. Seibert, M. and R. Pirorel, *Isolation of Photosystem II Reaction Center Complexes from Plants*, in *Photosynthesis Research Protocols. Methods in Molecular Biology (Methods and Protocols)*, R. Carpentier, Editor. 2011, Humana Press: Totowa, NJ. p. 17-27.
23. Morton, J., et al., *Structured near-infrared Magnetic Circular Dichroism spectra of the Mn4CaO5 cluster of PSII in T. vulcanus are dominated by Mn(IV) d-d 'spin-flip' transitions.* Biochimica et Biophysica Acta (BBA) - Bioenergetics, 2018. **1859**(2): p. 88-98.
24. Renger, T. and R.A. Marcus, *On the relation of protein dynamics and exciton relaxation in pigment–protein complexes: An estimation of the spectral density and a theory for the calculation of optical spectra.* The Journal of Chemical Physics, 2002. **116**(22): p. 9997-10019.
25. Adolphs, J. and T. Renger, *How proteins trigger excitation energy transfer in the FMO complex of green sulfur bacteria.* Biophys J, 2006. **91**(8): p. 2778-97.
26. Renger, T. and F. Muh, *Theory of excitonic couplings in dielectric media : foundation of Poisson-TrEsp method and application to photosystem I trimers.* Photosynth Res, 2012. **111**(1-2): p. 47-52.
27. Knox, R.S. and B.Q. Spring, *Dipole Strengths in the Chlorophylls.* Photochem Photobiol, 2003. **77**(5): p. 497-501.
28. Shao, Y., et al., *Advances in molecular quantum chemistry contained in the Q-Chem 4 program package.* Molecular Physics, 2014. **113**(2): p. 184-215.
29. Madjet Mel, A., F. Muh, and T. Renger, *Deciphering the Influence of Short-Range Electronic Couplings on Optical Properties of Molecular Dimers: Application to "Special Pairs" in Photosynthesis.* J Phys Chem B, 2009. **113**: p. 12603-12614.
30. Cupellini, L., et al., *Coupling to Charge Transfer States is the Key to Modulate the Optical Bands for Efficient Light Harvesting in Purple Bacteria.* J Phys Chem Lett, 2018. **9**(23): p. 6892-6899.

31. Kaufmann, C., et al., *Discrete pi-Stacks of Perylene Bisimide Dyes within Folda-Dimers: Insight into Long- and Short-Range Exciton Coupling.* J Am Chem Soc, 2018. **140**(31): p. 9986-9995.
32. Hestand, N.J. and F.C. Spano, *Expanded Theory of H- and J-Molecular Aggregates: The Effects of Vibronic Coupling and Intermolecular Charge Transfer.* Chem Rev, 2018. **118**(15): p. 7069-7163.
33. Cai, Z.L., et al., *Density Functional Theory for Charge Transfer: The Nature of the N-Bands of Porphyrins and Chlorophylls Revealed through CAM-B3LYP, CASPT2, and SAC-CI Calculations.* J. Phys. Chem. B, 2006. **110**: p. 15624-15632.

Acknowledgements

We thank Sindra Peterson Årsköld for taking the UV-vis data in Fig. 1, which is an extension of vis data previously presented in Ref [18]. We recognize the support of the Australian Research Council through grants DP110104565 and DP150103137 (E.K.). Financial support by the grant LIT-2017-4-SEE-009 and the district of Upper Austria is gratefully acknowledged (T.R.).

Supplementary Information

Non-conservative circular dichroism of photosystem II reaction centers: Is there an enhancement by a coupling with charge transfer states?

Dominik Lindorfer[1*], Frank Müh[1], Robin Purchase[2*], Elmars Krausz[2], Thomas Renger[1]

1. Institute for Theoretical Physics, Johannes Kepler University, Linz, Altenbergerstrasse 69, 4040 Linz, Austria.
2. Research School of Chemistry, Australian National University, Canberra, ACT 2601, Australia

Determination of Oscillator Strength of Pheophytin a and β-Carotene

Ab initio calculations often do not yield the magnitude of the transition dipole moments of pigments that are known from experiment and the calculated transition densities have to be re-scaled to obtain reliable excitonic couplings. Knox and Spring [Knox03] have performed an analysis of the dipole strength of the Q_y transition of Chl *a* in different solvents and have extrapolated a linear model fit to obtain the vacuum transition dipole moment. Since such an analysis is cumbersome and not yet available for Pheo *a* or β-carotene, we assume that the ratio of the transition dipole moments of either pigment with the Chl *a* Qy transition dipole moment is the same in a specific solvent with optical dielectric constant n_r^2 and in vacuum (denoted as vac below)

$$\mu_{0\to a}^{(\mathrm{vac})} = \frac{\mu_{0\to a}^{(n_r)}}{\mu_{\mathrm{Q_y}}^{(n_r)}}\,\mu_{\mathrm{Q_y}}^{(\mathrm{vac})} \qquad 1$$

For β-carotene the vacuum transition dipole moment of the $S_0 \to S_2$ transition is obtained by describing the absorption spectrum of the isolated pigment in 80% acetone by a superposition of four Gaussian functions to account for the vibrational transitions (see Figure S1, right), which are included as separate states in the exciton Hamiltonian. The oscillator strength of these Gaussians is compared to the oscillator strength in the absorption spectrum of Chl *a* in 80% acetone to obtain the appropriate transition dipole moments using eq. 1. The dipole strength of the low energy Q_y transition of Pheo *a* is obtained in the same way (Figure S2).

For the high-energy transitions of Pheo *a*, three different transitions with large oscillator strength are obtained by our quantum chemistry calculations in the Soret-band region between 345 nm and 440 nm. To estimate the vacuum dipole strengths of these transitions the calculated transition densities are scaled by a factor that is obtained from the ratio of the experimental absorption spectrum in the Soret-band region to that of the Q_y region (Figure S2). Thus, we assume that the influence of the solvent on the dipole strength of the high energy transitions is the same as for the Q_y transition.

The numerical values of the transition dipole strengths for Chl a were obtained previously and are given in Table S1. The transition dipole strengths for Pheo *a* and β-carotene that are obtained in the present work are given in Table S2 and Table S3. Absorption spectra of isolated pigments have been taken from the literature and were normalized to the experimental extinction coefficients [1-3]

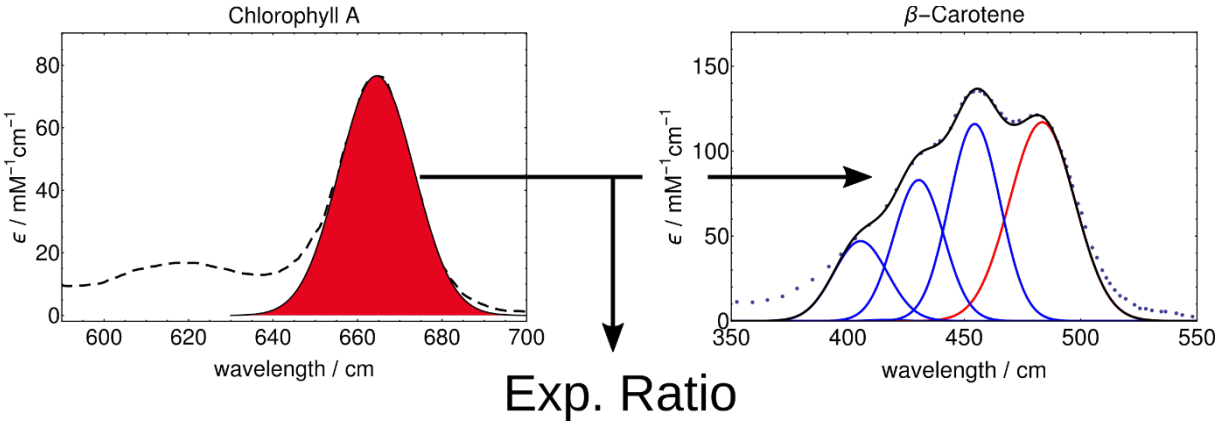

Figure S1: Absorption spectra of Chl a and β-carotene measured in 80% acetone. The Q_y absorption spectrum of Chla (left) is used to determine the experimental ratio between the oscillator strengths of Q_y and the β-carotene $S_0 \rightarrow S_2$ transition and its vibrational transitions using eq. 1 in the text. The β-carotene spectrum is described by four Gaussian functions where the red curve (right side) describes the 0-0 transition and the blue curves the excitation of intramolecular vibrational quanta. The experimental ratio Q_y / $S_0 \rightarrow S_2$ is used to scale the transition densities obtained by quantum chemical methods.

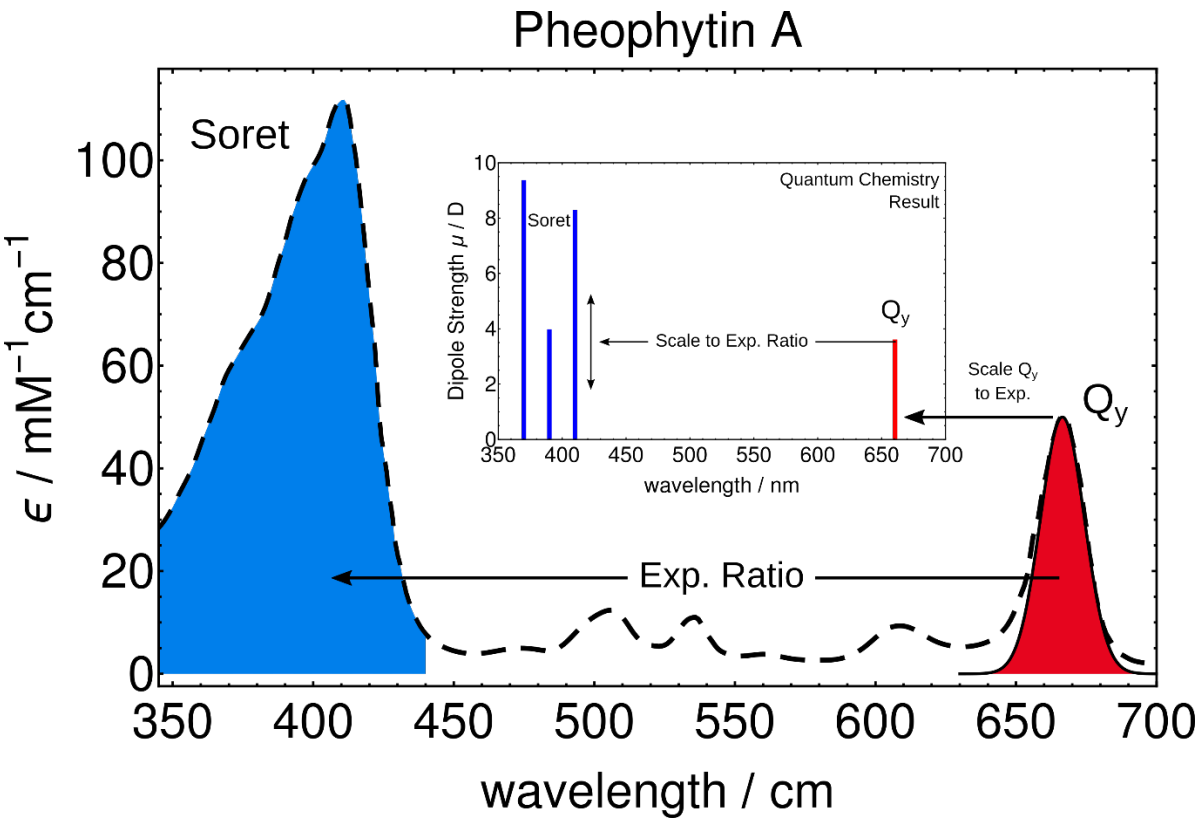

Figure S2: Absorption spectrum of Pheophytin a that is used to determine the vacuum transition dipole strength of the electronic transitions in the Soret region of the spectrum. The area under the Q_y transition (red) is compared to the area of Soret transitions (blue) to obtain an experimental ratio that is further used to scale the sum dipole strength of the calculated Soret transitions B_x, B_y and the N_{x+xy} by the same factor, as shown in the inset. The strength of the Pheo Q_y transition is determined beforehand using the Chl a absorption spectrum in Figure S1 in the same way as for β-carotene.

	CAM-B3LYP [D]	B3LYP [D]	BHHLYP [D]	HF-CIS [D]
Q_y	4.58	4.58	4.58	4.58
B_y	7.14	6.79	7.38	7.57
B_x	7.27	7.79	7.31	6.82
N_{x+xy}	4.13	3.76	3.61	3.91

Table S1: Chlorophyll a transition dipole strengths in Debye obtained using eq. 1

	CAM-B3LYP [D]	B3LYP [D]	BHHLYP [D]	HF-CIS [D]
Q_y	3.58	3.58	3.58	3.58
B_y	8.63	9.22	8.5	8.99
B_x	7.76	7.3	7.81	7.19
N_{x+xy}	4.18	3.72	4.32	4.41

Table S2: Pheophytin a transition dipole strengths in Debye obtained using eq. 1 and the procedure depicted in Figure S2.

	$\|\mu\|$ [D]	$FC_{0\to1}$	$FC_{0\to2}$	$FC_{0\to3}$
$S_0 \to S_2$	8.52	0.82	0.61	0.39

Table S3: β-carotene transition dipole strength in Debye and Franck-Condon factors for the vibrational Progression obtained using eq. 1 and the procedure depicted in Figure S1.

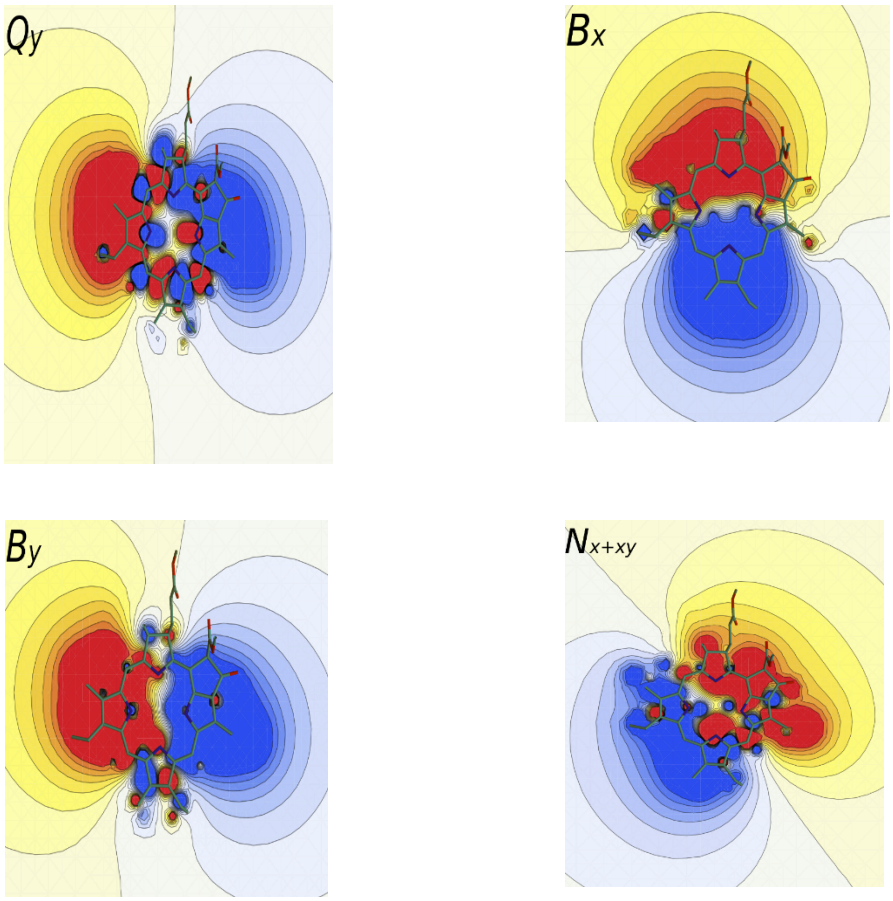

Figure S3: Electrostatic potentials from the transition densities of Pheo a obtained by TD-DFT with the CAM-B3LYP XC functional. The transitions have been assigned according to their dipole strengths and orientation of the transition dipole moment.

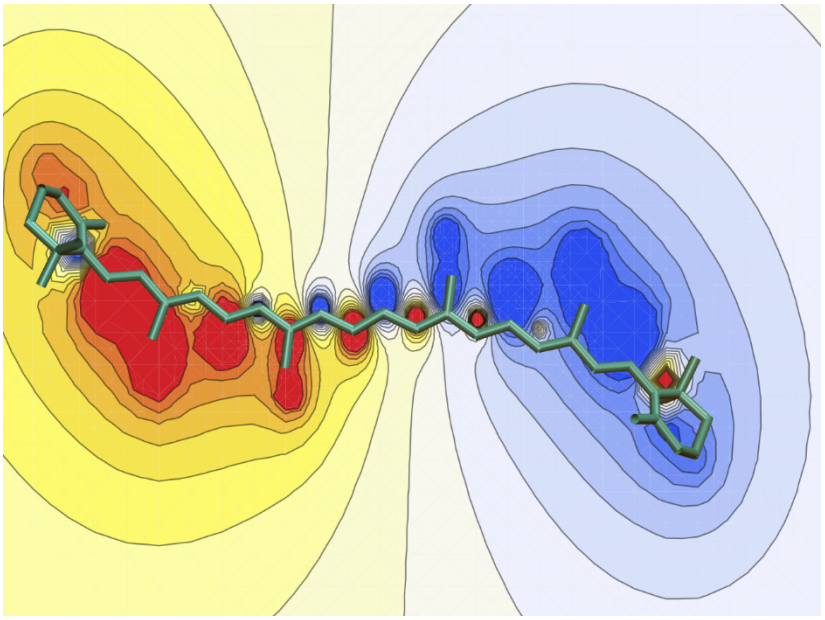

Figure S4: Electrostatic potentials of the transition densities of β-carotene obtained by TD-DFT with the CAM-B3LYP XC functional.

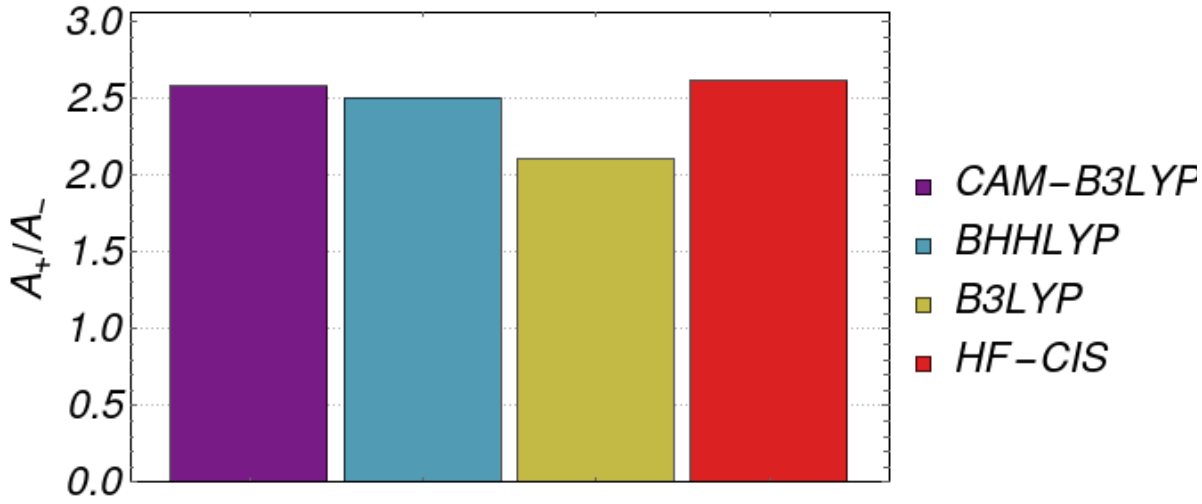

Figure S5: Non-conservativity of the CD spectrum obtained using excitonic couplings calculated with different quantum chemical methods.

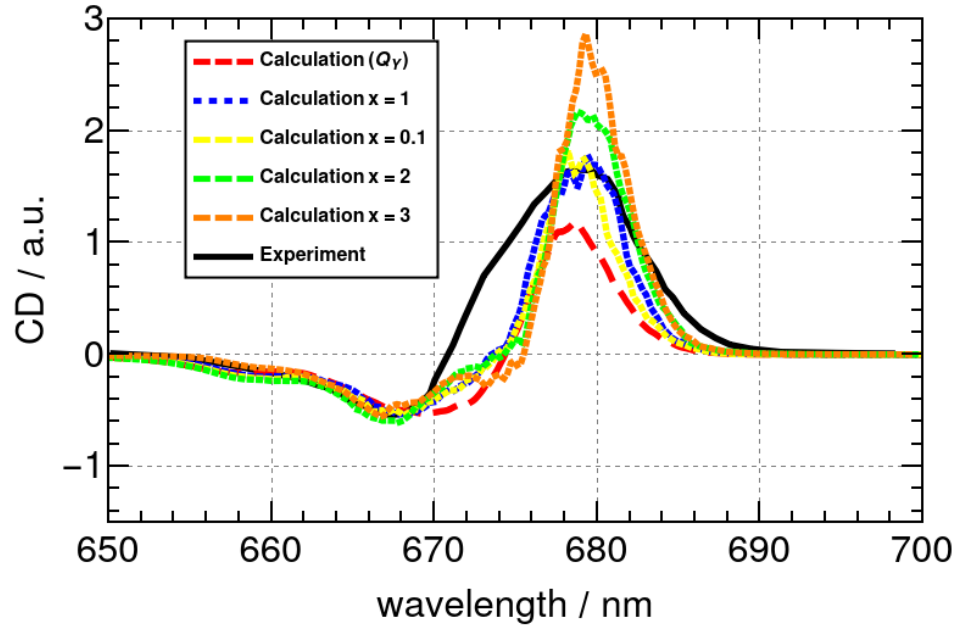

Figure S6: The low temperature (1.8 K) experimental CD spectrum (black solid line) is compared with calculations, where the enhancement factor x *of the excitonic coupling between the Qy transitions and high-energy transitions, as well as that between the latter, of the special pair pigments P_{D1} and P_{D2} is varied as indicated in the legend. The red dashed line contains the conservative CD spectrum calculated without including any coupling to high-energy transitions.*

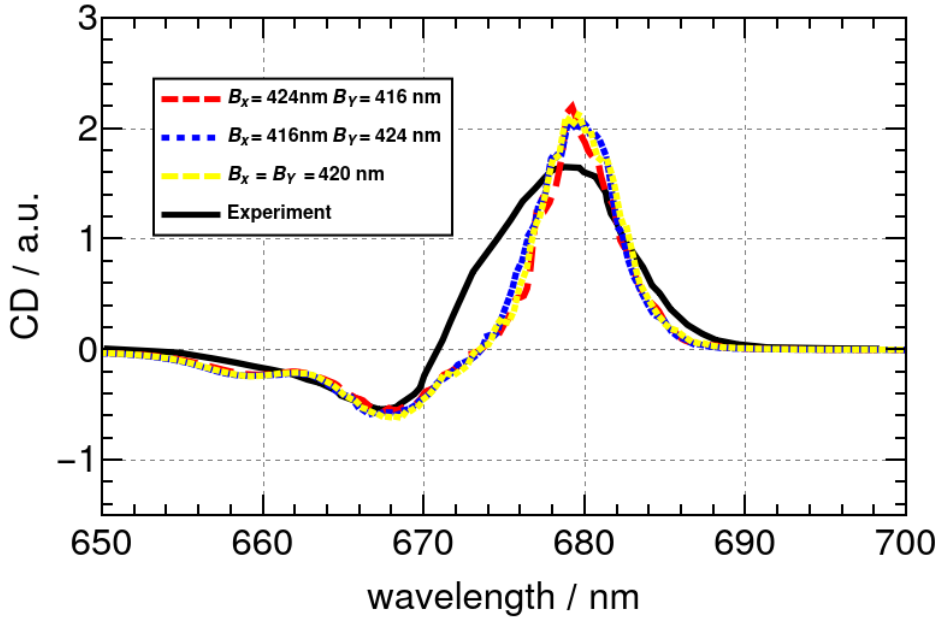

Figure S7: Dependence of the calculated CD spectrum on the energies of the high-energy B-transitions (colored lines). The transition energies are given in the figure legend, all other parameters as for the red dashed line in Fig. 1 of the main text. The black solid line shows the experimental spectrum for comparison.

Pigment *m*	Pigment *n*	$V_{mn}^{(Q_y)}$ (CAM-B3LYP) / cm^{-1}	$V_{mn}^{(Q_y)}$ (B3LYP) / cm^{-1}	$V_{mn}^{(Q_y)}$ (BHHLYP) / cm^{-1}	$V_{mn}^{(Q_y)}$ (HF-CIS) / cm^{-1}
P_{D1}	P_{D2}	82,40	72,12	82,77	94,74
P_{D1}	Chl_{D1}	-35,17	-30,27	-34,34	-43,27
P_{D1}	Chl_{D2}	-44,73	-43,00	-45,41	-50,15
P_{D1}	$Pheo_{D1}$	-3,00	3,04	-3,08	-2,18
P_{D1}	$Pheo_{D2}$	11,49	-12,49	11,54	9,24
P_{D1}	$Chlz_{D1}$	0,40	0,42	0,40	0,43
P_{D1}	$Chlz_{D2}$	0,62	0,56	0,62	0,55
P_{D2}	Chl_{D1}	-43,83	-43,93	-44,70	-48,18
P_{D2}	Chl_{D2}	-28,74	-24,75	-27,98	-35,50
P_{D2}	$Pheo_{D1}$	13,00	-14,60	13,12	10,11
P_{D2}	$Pheo_{D2}$	-2,31	2,39	-2,39	-1,20
P_{D2}	$Chlz_{D1}$	0,63	0,60	0,64	0,58
P_{D2}	$Chlz_{D2}$	0,63	0,64	0,63	0,68
Chl_{D1}	Chl_{D2}	4,05	3,95	4,18	3,91
Chl_{D1}	$Pheo_{D1}$	46,00	-42,02	46,21	53,15
Chl_{D1}	$Pheo_{D2}$	-2,25	2,35	-2,24	-2,29
Chl_{D1}	$Chlz_{D1}$	1,48	1,52	1,50	1,39
Chl_{D1}	$Chlz_{D2}$	-0,09	-0,07	-0,09	-0,09
Chl_{D2}	$Pheo_{D1}$	-2,46	2,58	-2,45	-2,53

Chl_{D2}	$Pheo_{D2}$	44,69	-40,68	44,78	49,52
Chl_{D2}	$Chlz_{D1}$	-0,05	-0,03	-0,05	-0,06
Chl_{D2}	$Chlz_{D2}$	1,67	1,65	1,67	1,55
$Pheo_{D1}$	$Pheo_{D2}$	1,55	1,68	1,53	1,73
$Pheo_{D1}$	$Chlz_{D1}$	-2,41	2,50	-2,41	-2,26
$Pheo_{D1}$	$Chlz_{D2}$	-0,15	0,16	-0,15	-0,15
$Pheo_{D2}$	$Chlz_{D1}$	-0,16	0,17	-0,16	-0,16
$Pheo_{D2}$	$Chlz_{D2}$	-2,41	2,50	-2,41	-2,28
$Chlz_{D1}$	$Chlz_{D2}$	0,13	0,13	0,13	0,13

Table S4: Excitonic couplings between Qy transitions obtained with the Poisson-Tresp method, using different quantum chemical methods, as described in the main text.

Pigment	**Site energy (nm)**	**Width (cm-1)**
PD1	666.5	180
PD2	666.5	180
ChlD1	676.5	180
ChlD2	668.5	180
PheoD1	668.5	180
PheoD2	673.5	180
ChlzD1	668.5	180
ChlzD2	663.5	180

Table S5: Site energies and widths (FWHM) for the Gaussian site energy distribution functions used in the simulation of the Qy absorption and CD spectra

References

1. Eijckelhoff, C. and J.P. Dekker, *A routine method to determine the chlorophyll a, pheophytin a and B -carotene contents of isolated Photosystem II reaction center complexes.* Photosynth Res, 1997. **52**: p. 69-73.
2. Sommer Márquez, A.E., et al., *Preparation of layered double hydroxide/chlorophyll a hybrid nano-antennae: a key step.* Dalton Transactions, 2014. **43**(27): p. 10521-10528.
3. Schlodder, E., *Introduction to optical methods in photosynthesis.* Photosynth Res, 2009. **101**(2-3): p. 93-104.

m	n	Vmn (CAM-B3LYP)	Vmn (B3LYP)	Vmn (BHHLYP)	Vmn (HF-CIS)
1	2	0	0	0	0
1	3	0	0	0	0
1	4	0	0	0	0
1	5	-35.1708	-30.273	-34.335	-43.2718
1	6	-41.6217	-71.4001	-42.6187	-11.8001
1	7	-149.917	-127.421	-149.993	-156.562
1	8	-49.3034	-59.7618	-36.1749	37.2983
1	9	-44.726	-43.0035	-45.4124	-50.148
1	10	-83.744	-75.2035	-87.8276	-85.5856
1	11	38.6618	54.0279	42.0979	18.3932
1	12	-2.78084	30.1588	-6.5841	13.2607
1	13	-2.99569	3.04435	-3.08267	-2.17596
1	14	-6.16833	-14.1795	-5.55354	-10.525
1	15	17.9147	14.386	17.5955	15.6695
1	16	9.46203	0.350621	10.2445	8.08753
1	17	11.488	-12.4912	11.5391	9.23863
1	18	32.3193	18.5849	33.6808	21.7684
1	19	30.8043	35.8019	30.211	39.3419
1	20	-7.00641	17.0284	-4.2145	-10.0392
1	21	0.397731	0.41797	0.399846	0.432615
1	22	1.0448	1.81776	0.971953	-0.010946
1	23	3.83307	3.52569	3.98011	4.1271
1	24	2.03995	2.13575	1.73166	-1.7653
1	25	158	158	158	158
1	26	273.252	238.412	272.236	310.61
1	27	-118.903	-151.253	-118.569	-12.6893
1	28	-25.4714	-17.5918	-13.7806	-7.82312
1	29	0.620519	0.564835	0.620769	0.546401
1	30	0.806038	0.557127	0.857489	1.02181
1	31	-1.26068	-1.47074	-1.31522	-1.11602
1	32	-0.398334	-0.589677	-0.283464	0.288909
1	33	2.05267	1.88511	2.05229	2.20345
1	34	1.68559	1.548	1.68528	1.80941
1	35	1.24995	1.14791	1.24971	1.34176
1	36	0.80762	0.741694	0.80747	0.866944
1	37	-0.0557	-0.042725	-0.04531	0.021517
1	38	-0.045739	-0.035084	-0.037207	0.017669
1	39	-0.033918	-0.026017	-0.027591	0.013102
1	40	-0.021915	-0.01681	-0.017827	0.008466
2	3	0	0	0	0
2	4	0	0	0	0
2	5	-54.1209	-56.6201	-53.0159	-56.6637
2	6	-62.911	-135.089	-64.8677	-18.0158
2	7	-221.962	-226.242	-228.55	-195.822
2	8	-73.539	-102.16	-55.1857	46.3007
2	9	-80.7116	-81.9867	-81.8031	-78.9625
2	10	-145.801	-136.273	-152.519	-138.139
2	11	66.7206	90.6947	71.7527	31.7745
2	12	-5.07441	61.2246	-11.9519	20.9451
2	13	-3.6895	8.47985	-4.12705	0.805927
2	14	-6.696	-21.9653	-6.5674	-5.69783

2	15	23.4893	-2.52824	24.1006	50.3614
2	16	11.4327	-7.36284	13.3238	7.84411
2	17	17.7793	-18.9411	18.0061	14.8013
2	18	49.5166	30.7366	51.9169	34.087
2	19	44.7624	47.0779	44.3129	66.3872
2	20	-11.4152	24.3044	-7.30591	-15.0655
2	21	0.502178	-0.061144	0.54957	1.23121
2	22	1.43061	1.81342	1.39709	0.944983
2	23	5.97838	6.3329	6.28798	6.08602
2	24	3.12652	3.48328	2.69374	-2.82124
2	25	209.984	138.308	214.824	304.842
2	26	387.624	422.256	382.778	492.982
2	27	104.772	195.132	109.728	-53.537
2	28	48.7788	120.539	40.3334	-64.1146
2	29	0.819148	0.301984	0.829001	1.24073
2	30	0.968564	-0.36565	1.07122	2.13638
2	31	-2.35957	-2.95853	-2.44621	-1.29379
2	32	-0.876608	-1.53726	-0.659213	0.136454
2	33	3.04607	2.32033	3.14775	3.87324
2	34	2.50135	1.90539	2.58484	3.18059
2	35	1.85486	1.41293	1.91678	2.35856
2	36	1.19847	0.91293	1.23848	1.52392
2	37	0.389227	0.898652	0.294444	-0.260601
2	38	0.319622	0.737948	0.241789	-0.213998
2	39	0.237015	0.547222	0.179298	-0.15869
2	40	0.153141	0.353573	0.115849	-0.102533
3	4	0	0	0	0
3	5	-30.7745	-16.16	-31.2023	-52.3492
3	6	-47.6161	-48.487	-50.2452	-18.6564
3	7	-142.627	-67.561	-148.616	-204.251
3	8	-50.1793	-20.8706	-39.6803	51.0274
3	9	-8.39291	7.41568	-9.20428	-23.5501
3	10	5.08247	23.5474	3.09458	-19.862
3	11	-5.63191	-3.95152	-0.007431	4.50954
3	12	-0.675857	12.634	0.782656	3.25512
3	13	-15.3468	14.5413	-15.8208	-14.0251
3	14	-49.1843	-3.61764	-54.2312	-25.8827
3	15	-86.7592	-91.5189	-88.4973	-95.3724
3	16	-1.82926	-30.2018	-8.46046	7.39821
3	17	-3.57853	7.20805	-3.49651	-0.945535
3	18	-12.3374	-4.00133	-13.3797	1.1789
3	19	-28.1731	-38.1768	-28.743	-24.7617
3	20	-2.89662	-13.4009	-5.27803	-3.34484
3	21	-2.78395	-2.66666	-2.89369	-2.63389
3	22	-4.31839	-4.35471	-4.58304	-4.65985
3	23	1.79049	1.3511	1.909	2.25703
3	24	-0.242108	-0.407371	-0.475707	0.101974
3	25	-215.052	-267.844	-230.836	-145.233
3	26	-231.908	-167.192	-241.418	-403.258
3	27	943.074	768.886	979.492	1115.19
3	28	81.4286	220.154	-7.64466	-35.1166
3	29	-1.91467	-1.92567	-1.97281	-1.88562

3	30	-3.27576	-3.72518	-3.38644	-2.48062
3	31	-1.98786	-0.949607	-2.19526	-3.20713
3	32	-1.73351	-1.33824	-1.6868	1.9483
3	33	-2.58645	-3.02612	-2.69307	-1.87994
3	34	-2.12392	-2.48496	-2.21147	-1.54375
3	35	-1.57498	-1.84272	-1.63991	-1.14476
3	36	-1.01763	-1.19062	-1.05958	-0.739659
3	37	2.7583	3.31297	2.92946	2.40902
3	38	2.26504	2.72052	2.40559	1.97822
3	39	1.67963	2.01739	1.78386	1.46694
3	40	1.08525	1.30348	1.15259	0.947825
4	5	-22.3422	-24.2662	-20.1026	26.5993
4	6	-29.8044	-67.6071	-27.8065	6.13949
4	7	-104.417	-114.607	-94.4962	108.281
4	8	-35.8584	-50.5988	-24.3809	-26.4732
4	9	-24.3614	-15.1968	-25.2019	28.0995
4	10	-64.8886	-22.8718	-72.1864	88.245
4	11	85.3037	32.3358	94.1843	-92.4721
4	12	17.5951	26.7648	9.97481	7.31263
4	13	-7.89516	7.83339	-6.64011	5.34999
4	14	-24.4374	-6.77446	-21.5797	10.9988
4	15	-36.2548	-35.9558	-28.8031	30.0877
4	16	1.19093	-13.4783	-0.879986	-3.75587
4	17	4.22835	-1.90207	4.86541	-4.26874
4	18	10.5595	6.43429	12.5193	-13.5154
4	19	-3.53429	-3.67458	-0.639534	-6.9716
4	20	-6.75272	0.760028	-6.35297	7.83951
4	21	-1.0948	-1.38434	-0.8667	0.730751
4	22	-1.55474	-1.71769	-1.25228	1.57444
4	23	2.15911	2.44837	2.15861	-2.2274
4	24	0.608069	0.754011	0.469897	0.581434
4	25	-151.448	-79.9174	-137.097	116.256
4	26	-171.538	10.9307	-163.464	187.268
4	27	350.908	321.22	274.468	-278.95
4	28	3.3477	96.8726	-20.2794	-53.3288
4	29	-0.583919	-0.716858	-0.419056	0.366341
4	30	-1.19313	-1.65904	-0.885021	0.235114
4	31	-2.04855	-1.22925	-2.02649	2.25259
4	32	-1.26303	-0.98785	-1.00015	-1.05338
4	33	-0.415024	-0.903345	-0.181299	-0.145124
4	34	-0.340806	-0.741801	-0.148878	-0.119172
4	35	-0.252723	-0.55008	-0.1104	-0.088371
4	36	-0.163291	-0.35542	-0.071332	-0.057099
4	37	2.19038	1.88785	1.99726	-1.99494
4	38	1.79868	1.55025	1.64009	-1.63819
4	39	1.3338	1.14958	1.2162	-1.21479
4	40	0.861802	0.742772	0.785819	-0.784906
5	6	0	0	0	0
5	7	0	0	0	0
5	8	0	0	0	0
5	9	4.04964	3.94689	4.17804	3.90552
5	10	7.85864	4.49766	8.23478	10.4821

5	11	-14.0895	-13.9405	-14.5041	-13.4192
5	12	-3.18842	-6.70259	-1.90056	1.47488
5	13	45.9996	-42.0197	46.2062	53.1464
5	14	75.0218	92.1195	72.5904	95.0589
5	15	-55.2222	-36.3882	-57.7416	-39.7359
5	16	-42.1491	17.9578	-45.6945	-40.617
5	17	-2.25309	2.354	-2.23735	-2.29105
5	18	-6.36164	-0.597315	-6.83129	-2.77915
5	19	-12.4652	-13.3096	-12.2119	-14.5268
5	20	-1.17539	-4.4396	-1.96451	-0.448538
5	21	1.48234	1.51665	1.50106	1.38644
5	22	2.2242	2.2493	2.43374	2.59627
5	23	-1.99444	-2.85748	-2.11035	-1.68498
5	24	-0.509483	-1.00875	-0.30573	0.3723
5	25	-43.8312	-43.9345	-44.7041	-48.1783
5	26	-93.9772	-100.2	-95.47	-85.0013
5	27	-23.4397	-11.795	-26.6945	-43.7628
5	28	-60.6231	-30.1283	-61.8947	75.28
5	29	-0.094888	-0.067685	-0.091811	-0.092792
5	30	0.019325	0.326743	-0.003234	-0.388585
5	31	1.42951	1.38284	1.48131	1.49591
5	32	0.675535	0.732764	0.5565	-0.563313
5	33	-0.375572	-0.299961	-0.364267	-0.449135
5	34	-0.308409	-0.246319	-0.299126	-0.368817
5	35	-0.2287	-0.182657	-0.221816	-0.273495
5	36	-0.147768	-0.118019	-0.14332	-0.176711
5	37	-0.544566	-0.576902	-0.538142	-0.599575
5	38	-0.447182	-0.473736	-0.441907	-0.492354
5	39	-0.331606	-0.351297	-0.327694	-0.365103
5	40	-0.214259	-0.226981	-0.211731	-0.235902
6	7	0	0	0	0
6	8	0	0	0	0
6	9	7.66498	4.20525	8.0554	10.5821
6	10	14.1649	3.06889	15.1419	21.4818
6	11	-21.9184	-24.7892	-22.9689	-15.1989
6	12	-4.63561	-12.9471	-2.62654	-0.638626
6	13	85.1836	-78.4637	85.3065	97.3528
6	14	156.877	178.716	152.36	182.458
6	15	-78.007	-22.5682	-82.6381	-65.2726
6	16	-85.5158	48.9541	-87.8645	-81.7051
6	17	-3.66441	2.9545	-3.70414	-4.4103
6	18	-10.2619	1.53685	-11.1959	-7.22854
6	19	-18.8409	-23.028	-19.0219	-19.817
6	20	-1.42106	-6.88199	-2.78473	1.90235
6	21	2.83882	2.66253	2.82089	2.60056
6	22	4.17221	2.91653	4.44897	4.48417
6	23	-4.47852	-7.69854	-4.71809	-1.00827
6	24	-1.24609	-3.21612	-0.83313	-0.151937
6	25	-75.3729	-73.822	-79.3371	-74.8191
6	26	-158.78	-166.137	-166.78	-132.232
6	27	-28.274	-14.6085	-35.4911	-61.843
6	28	-121.779	-49.54	-130.249	148.162

6	29	-0.097907	-0.30362	-0.108002	0.137814
6	30	0.121171	0.317175	0.064654	-0.118744
6	31	2.34762	2.60878	2.45959	2.15768
6	32	1.13094	1.30005	0.941201	-0.932017
6	33	-0.200164	-0.553137	-0.305272	0.136702
6	34	-0.164369	-0.45422	-0.250681	0.112256
6	35	-0.121887	-0.336825	-0.185891	0.083243
6	36	-0.078754	-0.217631	-0.120109	0.053785
6	37	-1.01722	-1.92758	-1.0008	-0.065396
6	38	-0.835312	-1.58287	-0.821829	-0.053701
6	39	-0.619423	-1.17377	-0.609424	-0.039822
6	40	-0.400224	-0.758403	-0.393763	-0.02573
7	8	0	0	0	0
7	9	-14.8925	-14.5904	-15.3188	-14.3381
7	10	-22.3763	-25.2337	-23.336	-15.8431
7	11	-13.1088	-3.86729	-13.564	-22.5319
7	12	-9.86673	-5.54451	-9.29141	10.8555
7	13	-21.4609	36.4906	-23.1685	-18.4085
7	14	-6.05449	-75.2796	-3.10277	16.4173
7	15	71.5286	72.5011	77.446	96.0692
7	16	11.6604	-2.31523	19.7767	-21.5984
7	17	4.11801	-4.46793	4.32418	2.96205
7	18	8.54295	11.7604	8.52352	10.0512
7	19	-9.83084	-3.40586	-10.0394	-10.2135
7	20	-8.5918	2.5365	-9.03119	-9.18625
7	21	-0.364186	-0.631339	-0.286804	0.181679
7	22	-1.45003	-3.67077	-1.33114	2.00587
7	23	-8.36168	-6.48074	-9.12524	-10.0771
7	24	-4.06185	-3.76557	-3.54823	3.57825
7	25	19.8662	37.4534	22.4316	2.03568
7	26	42.5209	76.3599	47.0604	4.97048
7	27	10.1175	17.1514	16.7068	13.705
7	28	77.8941	35.785	85.8983	-70.0692
7	29	-0.998997	-0.857632	-1.02922	-0.97953
7	30	-1.52066	-1.2255	-1.58136	-1.82768
7	31	1.0853	0.76839	1.15398	1.3807
7	32	0.09324	0.031868	-0.013809	-0.104315
7	33	-1.47068	-0.524046	-1.46983	-2.14114
7	34	-1.20768	-0.430332	-1.20698	-1.75824
7	35	-0.895551	-0.319111	-0.895033	-1.30382
7	36	-0.578637	-0.206185	-0.578302	-0.842428
7	37	-3.62896	-3.12277	-3.74957	-4.07394
7	38	-2.98	-2.56433	-3.07904	-3.3454
7	39	-2.20981	-1.90157	-2.28325	-2.48077
7	40	-1.42781	-1.22865	-1.47526	-1.60289
8	9	-3.49508	-6.97659	-2.13143	1.72474
8	10	-4.74848	-12.9148	-2.6811	-0.454942
8	11	-9.81434	-5.86417	-9.23021	10.7217
8	12	-4.68075	-4.53026	-3.20955	-3.24591
8	13	-11.8529	1.1524	-9.55581	10.6848
8	14	-9.63205	0.158944	-6.76725	5.57151
8	15	16.288	20.4296	11.2518	-11.0018

8	16	0.552385	5.91812	-0.28522	6.23524
8	17	0.76347	-1.64648	0.409059	0.036093
8	18	0.9302	6.4957	-0.158591	-1.70924
8	19	-8.49065	-6.95989	-7.6968	8.37967
8	20	-3.808	-0.225714	-3.44313	2.75856
8	21	1.51368	0.511228	1.62655	-1.84397
8	22	1.77527	-0.666455	2.15399	-3.99019
8	23	-6.49529	-4.80932	-6.1798	5.76952
8	24	-2.59279	-2.42669	-1.78642	-1.61424
8	25	-6.70432	15.0752	-8.714	14.7247
8	26	-14.1208	52.8197	-18.8695	25.2607
8	27	-3.76297	27.9534	-5.02733	11.3196
8	28	7.0763	29.1641	0.1985	-8.07731
8	29	-0.418328	-0.510147	-0.332099	0.297012
8	30	-0.569046	-0.564674	-0.449576	0.658446
8	31	1.03376	0.966109	1.00646	-1.05615
8	32	0.326869	0.29938	0.248929	0.284058
8	33	-0.188592	-0.23254	-0.044423	0.266145
8	34	-0.154866	-0.190955	-0.036479	0.218551
8	35	-0.114841	-0.141602	-0.027051	0.162065
8	36	-0.074201	-0.091493	-0.017478	0.104714
8	37	-1.72807	-1.88886	-1.45425	1.48407
8	38	-1.41904	-1.55108	-1.19419	1.21868
8	39	-1.05229	-1.1502	-0.885546	0.903705
8	40	-0.679906	-0.743169	-0.572172	0.583905
9	10	0	0	0	0
9	11	0	0	0	0
9	12	0	0	0	0
9	13	-2.46148	2.57759	-2.44935	-2.53383
9	14	-6.99812	-0.929465	-7.50048	-3.40878
9	15	-12.7926	-13.8987	-12.5542	-15.2119
9	16	-1.09116	-4.72347	-1.94793	-0.229798
9	17	44.6936	-40.6768	44.7752	49.5177
9	18	77.5952	91.2249	75.385	96.0975
9	19	-49.4505	-30.3244	-51.5051	-30.9292
9	20	-44.0982	19.4554	-46.4207	-44.6935
9	21	-0.049919	-0.030368	-0.049802	-0.057807
9	22	0.046478	0.335067	0.017441	-0.360763
9	23	1.39928	1.34707	1.44984	1.46167
9	24	0.652376	0.726532	0.532671	-0.53198
9	25	-28.7378	-24.7502	-27.9837	-35.4998
9	26	-43.8211	-49.5739	-42.3894	-41.1781
9	27	-40.3881	-25.5461	-41.0054	-58.7617
9	28	-23.5078	-24.2899	-20.2508	23.9036
9	29	1.66649	1.65303	1.66791	1.55455
9	30	2.27378	2.42044	2.43921	2.44532
9	31	-1.27913	-2.32069	-1.3723	-0.892238
9	32	-0.344793	-0.733416	-0.220498	0.351004
9	33	0.67906	0.640993	0.680591	0.697331
9	34	0.557625	0.526365	0.558882	0.572628
9	35	0.413505	0.390324	0.414437	0.42463
9	36	0.267175	0.252198	0.267777	0.274364

9	37	6.89978	6.87524	6.95256	7.65324
9	38	5.6659	5.64575	5.70925	6.28462
9	39	4.20153	4.18659	4.23367	4.66034
9	40	2.71471	2.70505	2.73547	3.01116
10	11	0	0	0	0
10	12	0	0	0	0
10	13	-4.06552	3.41998	-4.10206	-4.77953
10	14	-11.593	1.34258	-12.6268	-7.80938
10	15	-21.1434	-25.3997	-21.2629	-22.5461
10	16	-1.78319	-7.69603	-3.33465	1.74354
10	17	75.4429	-68.0775	75.3257	86.3811
10	18	138.618	157.095	134.174	169.854
10	19	-76.1895	-22.8082	-79.7705	-64.6036
10	20	-79.3062	42.1474	-81.1994	-81.1862
10	21	-0.102809	-0.29205	-0.114181	0.100934
10	22	0.03633	0.228891	-0.028795	-0.207241
10	23	2.24373	2.5157	2.34238	2.02337
10	24	1.03481	1.25346	0.843514	-0.816584
10	25	-33.8449	-60.9524	-34.3534	-7.30383
10	26	-48.885	-118.665	-49.2919	-5.31981
10	27	-52.3352	-56.9073	-54.5205	-20.8708
10	28	-28.2216	-60.068	-25.0101	2.6219
10	29	2.73831	2.5996	2.69918	2.42982
10	30	3.54083	2.50591	3.76818	3.53647
10	31	-3.6901	-7.32952	-3.89513	0.135182
10	32	-1.34068	-3.14182	-1.02776	0.049747
10	33	1.07264	0.729899	1.07406	1.30284
10	34	0.880822	0.599372	0.881988	1.06986
10	35	0.65317	0.444462	0.654035	0.793347
10	36	0.422029	0.287178	0.422587	0.5126
10	37	13.6103	18.7617	13.7324	8.46589
10	38	11.1764	15.4066	11.2767	6.95195
10	39	8.28781	11.4247	8.36216	5.15519
10	40	5.35495	7.38176	5.40299	3.33089
11	12	0	0	0	0
11	13	3.94682	-4.38696	4.14725	2.61376
11	14	8.28756	11.3939	8.27356	9.21735
11	15	-9.09076	-2.54292	-9.27541	-10.0814
11	16	-8.41234	2.69698	-8.8485	-8.85677
11	17	-24.2287	36.8467	-26.1183	-20.8168
11	18	-15.8436	-81.741	-14.0936	-3.90277
11	19	79.3272	76.7511	84.9497	93.1201
11	20	18.4507	-2.65013	26.3513	-8.04506
11	21	-0.9249	-0.794401	-0.954286	-0.910518
11	22	-1.40904	-1.09674	-1.45636	-1.7217
11	23	1.09474	0.776023	1.16351	1.35593
11	24	0.124361	0.077028	0.017231	-0.117496
11	25	-133.785	-115.053	-133.64	-138.01
11	26	-205.817	-209.349	-209.241	-173.432
11	27	-138.56	-71.4977	-143.373	-193.508
11	28	-95.6585	-101.323	-86.0199	96.2226
11	29	-0.134088	-0.417933	-0.054623	0.324033

11	30	-1.1795	-3.69354	-1.03063	2.4599
11	31	-9.57049	-7.88208	-10.4619	-11.395
11	32	-4.53315	-4.34156	-3.95962	4.0434
11	33	-1.19568	-1.31298	-1.23362	-0.829174
11	34	-0.981859	-1.07818	-1.01301	-0.680894
11	35	-0.728093	-0.799522	-0.751196	-0.504914
11	36	-0.470438	-0.51659	-0.485366	-0.326237
11	37	20.8292	17.6325	21.8479	23.238
11	38	17.1043	14.4793	17.9409	19.0824
11	39	12.6837	10.7371	13.304	14.1505
11	40	8.19522	6.93748	8.59602	9.14296
12	13	0.619165	-1.5603	0.275631	0.239977
12	14	0.536579	6.39512	-0.575951	-1.35945
12	15	-8.96316	-7.01196	-8.25701	9.24702
12	16	-3.9221	-0.273715	-3.64016	2.79014
12	17	-14.3811	4.50295	-12.0847	12.5425
12	18	-18.2959	-9.27051	-15.3316	18.2036
12	19	21.4259	21.9751	15.6185	-9.9328
12	20	6.96747	3.61643	5.51957	-3.09952
12	21	-0.405583	-0.484055	-0.328368	0.299988
12	22	-0.570627	-0.538339	-0.463565	0.671554
12	23	1.01242	0.935713	0.980811	-1.01055
12	24	0.309095	0.300867	0.226268	0.251711
12	25	-44.4249	-54.9229	-32.6146	33.4182
12	26	-68.1931	-95.506	-50.7035	40.7559
12	27	-50.2403	-20.2867	-39.8508	49.9878
12	28	-33.4875	-43.4608	-22.6419	-23.4683
12	29	1.50128	0.549465	1.57828	-1.74134
12	30	1.43717	-0.853592	1.79338	-3.78691
12	31	-7.37766	-5.34179	-7.01476	6.69218
12	32	-3.23419	-2.68501	-2.36338	-2.30778
12	33	-0.209892	-0.525918	-0.097097	-0.04786
12	34	-0.172357	-0.431869	-0.079733	-0.039301
12	35	-0.127811	-0.320251	-0.059126	-0.029144
12	36	-0.082582	-0.206922	-0.038203	-0.018831
12	37	14.6437	12.7661	13.185	-13.6022
12	38	12.025	10.4832	10.8271	-11.1697
12	39	8.91709	7.77375	8.02883	-8.28288
12	40	5.76154	5.0228	5.18762	-5.35176
13	14	0	0	0	0
13	15	0	0	0	0
13	16	0	0	0	0
13	17	1.55038	1.68072	1.52619	1.73279
13	18	4.02545	-1.11262	4.21368	2.40987
13	19	6.21991	-7.37285	6.00498	7.63793
13	20	0.296734	-2.69113	0.693998	-0.157008
13	21	-2.41484	2.50419	-2.41136	-2.26059
13	22	-4.08104	4.31433	-4.02783	-3.55855
13	23	-0.317946	-0.128347	-0.379022	-0.961008
13	24	-1.5444	1.08075	-1.57534	1.72897
13	25	13.0039	-14.596	13.1181	10.1125
13	26	21.3076	-23.5613	21.5904	16.5632

13	27	-3.43337	6.15122	-2.94063	0.45606
13	28	10.6792	-4.26172	11.6089	-9.60121
13	29	-0.151487	0.160975	-0.15386	-0.154683
13	30	-0.324773	0.501791	-0.322672	-0.114136
13	31	-0.724936	0.641203	-0.755363	-0.790607
13	32	-0.43632	0.416782	-0.383597	0.382902
13	33	-4.11436	4.29742	-4.10099	-3.78575
13	34	-3.3786	3.52892	-3.36762	-3.10875
13	35	-2.50538	2.61686	-2.49724	-2.30528
13	36	-1.61879	1.69081	-1.61353	-1.4895
13	37	0.500352	-0.499266	0.513973	0.371734
13	38	0.410875	-0.409983	0.42206	0.305257
13	39	0.304683	-0.304021	0.312977	0.226362
13	40	0.196863	-0.196435	0.202222	0.146258
14	15	0	0	0	0
14	16	0	0	0	0
14	17	4.13746	-1.3757	4.30733	2.62968
14	18	10.7167	2.55067	11.8842	4.47939
14	19	16.5857	2.33996	17.2524	8.95549
14	20	0.694965	1.46375	1.9731	-1.23614
14	21	-5.44817	-3.125	-5.59755	-3.63953
14	22	-9.31223	-4.79909	-9.51274	-5.72909
14	23	-1.50989	0.665802	-1.84152	-1.27894
14	24	-3.82288	-1.15624	-3.98166	2.72794
14	25	37.3408	22.7718	38.9952	24.542
14	26	60.3992	39.7035	63.1774	40.0193
14	27	-12.9247	-2.12505	-12.8199	3.49553
14	28	28.1309	11.5027	31.1702	-31.9573
14	29	-0.318811	-0.51119	-0.306666	-0.45361
14	30	-0.696057	-1.35395	-0.659964	-0.426848
14	31	-1.567	-1.23625	-1.6238	-1.72082
14	32	-0.944397	-0.876507	-0.819072	0.86322
14	33	-9.24874	-6.39478	-9.39203	-6.52282
14	34	-7.5948	-5.25121	-7.71247	-5.35636
14	35	-5.6319	-3.89402	-5.71915	-3.97198
14	36	-3.6389	-2.51602	-3.69528	-2.56639
14	37	0.590912	2.84813	0.415445	1.6521
14	38	0.48524	2.3388	0.341152	1.35666
14	39	0.359828	1.73433	0.25298	1.00602
14	40	0.232493	1.12059	0.163456	0.650016
15	16	0	0	0	0
15	17	5.73795	-6.90721	5.51143	7.33828
15	18	15.3183	0.804606	16.0057	7.96479
15	19	32.7774	38.4792	31.4707	40.7695
15	20	3.93619	12.692	5.93113	1.36056
15	21	-4.89629	-6.17424	-4.76041	-6.00993
15	22	-8.9165	-12.7635	-8.82387	-8.91121
15	23	-4.50311	-2.40403	-4.68169	-7.03097
15	24	-4.82805	-3.88619	-4.52087	5.67053
15	25	34.6706	40.8992	33.9723	44.2669
15	26	51.9483	57.0855	51.1889	74.6999
15	27	-27.8737	-38.4346	-28.3614	-21.8029

15	28	-0.424628	-1.146	2.44723	-16.9807
15	29	0.415292	0.322464	0.416369	0.292416
15	30	0.599071	0.474076	0.644239	0.486434
15	31	-0.053083	-0.534108	-0.020208	-0.430278
15	32	0.114854	-0.188818	0.150833	0.149245
15	33	-6.56561	-8.28553	-6.3047	-8.72909
15	34	-5.39149	-6.80384	-5.17724	-7.16808
15	35	-3.99804	-5.04536	-3.83916	-5.31546
15	36	-2.58323	-3.25993	-2.48057	-3.43445
15	37	-4.70484	-4.77479	-4.67349	-4.12193
15	38	-3.86348	-3.92092	-3.83774	-3.38481
15	39	-2.86495	-2.90754	-2.84586	-2.50999
15	40	-1.85111	-1.87863	-1.83878	-1.62177
16	17	0.177882	-2.62521	0.567083	-0.243442
16	18	0.443579	0.978663	1.64931	-1.02463
16	19	2.71377	13.1539	4.70275	0.232802
16	20	0.54859	4.5304	1.04046	0.501766
16	21	0.5901	-3.06177	0.223393	0.573191
16	22	0.839189	-5.73682	0.089816	0.98304
16	23	-0.732632	-0.413136	-0.993789	-0.674485
16	24	0.045015	-1.57268	-0.199372	-0.261584
16	25	-8.30619	19.9328	-5.19921	-11.1539
16	26	-14.5855	30.2286	-9.78071	-17.8017
16	27	-2.0886	-12.9179	-4.95749	-4.13151
16	28	-14.585	3.09871	-13.589	18.3533
16	29	0.301201	-0.047118	0.314319	0.330313
16	30	0.554475	-0.256187	0.575965	0.331424
16	31	0.806509	-0.562438	0.794738	1.0672
16	32	0.529758	-0.333065	0.460798	-0.53328
16	33	1.7797	-4.65343	1.26987	1.60436
16	34	1.46144	-3.82126	1.04278	1.31745
16	35	1.08372	-2.83364	0.77327	0.976954
16	36	0.70022	-1.83088	0.499628	0.631233
16	37	-2.24101	-0.634748	-2.45565	-2.12364
16	38	-1.84025	-0.521237	-2.01651	-1.74387
16	39	-1.36463	-0.386521	-1.49534	-1.29316
16	40	-0.881722	-0.249741	-0.966172	-0.835543
17	18	0	0	0	0
17	19	0	0	0	0
17	20	0	0	0	0
17	21	-0.160437	0.172761	-0.161446	-0.156287
17	22	-0.32817	0.498748	-0.324419	-0.121293
17	23	-0.676609	0.59302	-0.705218	-0.748287
17	24	-0.41321	0.39626	-0.363538	0.364734
17	25	-2.31195	2.3891	-2.39282	-1.20173
17	26	-3.34969	7.71386	-3.73063	1.23717
17	27	-15.189	14.7185	-15.4907	-13.0085
17	28	-7.8246	7.4972	-6.53982	5.37763
17	29	-2.4075	2.4956	-2.4085	-2.2807
17	30	-4.1048	4.31446	-4.07556	-3.68385
17	31	-0.217956	-0.16646	-0.268179	-0.713091
17	32	-1.58096	1.10176	-1.62148	1.77421

17	33	-0.596102	0.582348	-0.595777	-0.615101
17	34	-0.489502	0.478208	-0.489235	-0.505104
17	35	-0.362988	0.354613	-0.36279	-0.374558
17	36	-0.234535	0.229124	-0.234408	-0.242011
17	37	-3.66571	3.66078	-3.6642	-3.59694
17	38	-3.01018	3.00613	-3.00894	-2.95371
17	39	-2.23219	2.22918	-2.23127	-2.19031
17	40	-1.44227	1.44033	-1.44167	-1.41521
18	19	0	0	0	0
18	20	0	0	0	0
18	21	-0.344736	-0.437441	-0.338852	-0.390217
18	22	-0.705311	-1.19524	-0.676702	-0.357511
18	23	-1.46507	-1.11634	-1.52412	-1.58376
18	24	-0.891664	-0.789414	-0.776927	0.791755
18	25	-4.00141	-15.3663	-3.22968	-9.21848
18	26	-4.34241	-24.6711	-3.79275	-6.81981
18	27	-48.8956	-2.77538	-53.7371	-21.3897
18	28	-23.9742	-5.71672	-21.0453	9.66565
18	29	-5.54091	-3.0134	-5.71891	-3.69865
18	30	-9.51844	-4.42034	-9.78957	-6.15364
18	31	-1.52318	1.66191	-1.95852	-0.220751
18	32	-4.02714	-0.688996	-4.23621	2.61116
18	33	-1.34843	-1.02094	-1.36175	-1.26279
18	34	-1.10729	-0.838367	-1.11823	-1.03697
18	35	-0.821108	-0.621688	-0.82922	-0.768959
18	36	-0.530538	-0.401687	-0.535778	-0.496843
18	37	-7.43598	-6.41437	-7.46033	-6.03592
18	38	-6.10622	-5.2673	-6.12621	-4.95653
18	39	-4.52804	-3.90595	-4.54287	-3.67549
18	40	-2.92567	-2.52372	-2.93526	-2.37482
19	20	0	0	0	0
19	21	0.154909	0.069036	0.159075	0.053032
19	22	0.252124	0.107873	0.306618	0.205568
19	23	-0.129472	-0.530869	-0.103753	-0.558918
19	24	0.015227	-0.272364	0.054483	0.218255
19	25	23.9253	20.8398	22.9936	22.2134
19	26	34.2321	8.58981	34.2575	62.2417
19	27	-88.1712	-95.2986	-90.8651	-96.3644
19	28	-38.3792	-37.4108	-30.9452	33.1635
19	29	-5.17244	-6.51141	-5.02235	-6.30254
19	30	-9.38404	-13.9472	-9.20398	-8.49759
19	31	-7.40858	-4.95134	-7.72143	-10.1626
19	32	-6.3144	-5.32788	-5.76078	6.81935
19	33	-0.50056	-0.857786	-0.473929	-0.776615
19	34	-0.411046	-0.70439	-0.389177	-0.637734
19	35	-0.304809	-0.522337	-0.288593	-0.472909
19	36	-0.196945	-0.337495	-0.186467	-0.305558
19	37	-2.16789	-2.58845	-1.91097	-5.42264
19	38	-1.78021	-2.12556	-1.56923	-4.45292
19	39	-1.32011	-1.5762	-1.16366	-3.30204
19	40	-0.852953	-1.01842	-0.751868	-2.13353
20	21	0.244718	-0.105291	0.245712	0.271516

20	22	0.472653	-0.325138	0.482094	0.283615
20	23	0.698566	-0.528312	0.679039	0.931175
20	24	0.465493	-0.334996	0.400976	-0.478938
20	25	10.9007	2.00836	12.0039	8.34967
20	26	14.5262	-4.72139	16.9664	10.3873
20	27	-2.31662	-31.2029	-9.28822	4.4855
20	28	0.6755	-13.6509	-1.49734	-3.28904
20	29	0.397579	-3.16919	0.022912	0.40213
20	30	0.590336	-6.06199	-0.137642	1.03521
20	31	-1.48268	-0.939533	-1.92473	-1.61334
20	32	-0.295297	-1.91695	-0.532328	-0.031807
20	33	0.51447	-0.584618	0.456256	0.684985
20	34	0.422468	-0.480072	0.374665	0.56249
20	35	0.31328	-0.355995	0.277831	0.417112
20	36	0.202417	-0.230017	0.179513	0.269506
20	37	2.15417	-3.0531	1.89735	1.64563
20	38	1.76894	-2.50712	1.55805	1.35134
20	39	1.31175	-1.85914	1.15537	1.00208
20	40	0.847555	-1.20124	0.746509	0.647471
21	22	0	0	0	0
21	23	0	0	0	0
21	24	0	0	0	0
21	25	0.633315	0.596574	0.635429	0.57985
21	26	0.904637	0.457968	0.910262	1.26627
21	27	-1.73836	-1.78059	-1.78434	-1.62929
21	28	-0.448703	-0.633219	-0.296251	0.250637
21	29	0.129311	0.133835	0.129553	0.133724
21	30	0.224899	0.29218	0.227142	0.164485
21	31	0.215752	0.157983	0.224763	0.263375
21	32	0.160822	0.141264	0.147153	-0.152217
21	33	52.8858	50.091	53.1184	56.4085
21	34	43.4283	41.1333	43.6193	46.3211
21	35	32.2041	30.5022	32.3457	34.3492
21	36	20.8078	19.7082	20.8994	22.1938
21	37	-0.412205	-0.416775	-0.412995	-0.363117
21	38	-0.338491	-0.342244	-0.33914	-0.298181
21	39	-0.251007	-0.25379	-0.251488	-0.221115
21	40	-0.162181	-0.163979	-0.162492	-0.142868
22	23	0	0	0	0
22	24	0	0	0	0
22	25	0.952358	0.807318	1.00557	1.08457
22	26	1.30699	0.213974	1.40717	2.19715
22	27	-3.0242	-3.52424	-3.08593	-2.06548
22	28	-0.906316	-1.44316	-0.599382	0.064392
22	29	0.227162	0.287897	0.229952	0.17501
22	30	0.393229	0.581989	0.400361	0.199407
22	31	0.343794	0.210622	0.354697	0.418512
22	32	0.266299	0.235522	0.244644	-0.223785
22	33	102.664	102.52	103.675	104.615
22	34	84.3048	84.1865	85.135	85.9069
22	35	62.5159	62.4282	63.1315	63.7039
22	36	40.393	40.3363	40.7908	41.1606

22	37	-0.587714	-0.417296	-0.603321	-0.767292
22	38	-0.482614	-0.342672	-0.49543	-0.630078
22	39	-0.357881	-0.254107	-0.367384	-0.467232
22	40	-0.231235	-0.164184	-0.237376	-0.30189
23	24	0	0	0	0
23	25	-0.887554	-1.13686	-0.926295	-0.72972
23	26	-1.80747	-2.52553	-1.86871	-0.687012
23	27	-2.10044	-1.16891	-2.30891	-3.21953
23	28	-1.81909	-1.17113	-1.7675	1.89444
23	29	0.186729	0.131252	0.194997	0.234613
23	30	0.303418	0.172885	0.316074	0.378113
23	31	-0.094701	-0.145866	-0.099082	0.041568
23	32	0.041764	-0.019539	0.054985	-0.127062
23	33	7.01891	7.03062	7.11722	-0.43267
23	34	5.76373	5.77335	5.84446	-0.355296
23	35	4.27407	4.2812	4.33394	-0.263469
23	36	2.76158	2.76619	2.80026	-0.170233
23	37	1.00084	1.04306	1.03491	0.947078
23	38	0.821861	0.856531	0.849839	0.777714
23	39	0.609448	0.635157	0.630195	0.576711
23	40	0.393779	0.41039	0.407184	0.372626
24	25	-0.151431	-0.380905	-0.060411	0.053102
24	26	-0.47643	-1.21275	-0.293288	-0.22895
24	27	-1.7366	-1.40106	-1.66896	1.86816
24	28	-1.07156	-0.917786	-0.814186	-0.840812
24	29	0.151527	0.127826	0.140522	-0.147915
24	30	0.252814	0.217539	0.235789	-0.215499
24	31	0.05066	-0.012377	0.064742	-0.134032
24	32	0.094322	0.049187	0.09228	0.116693
24	33	35.1237	16.7808	36.2286	-37.2971
24	34	28.8426	13.7799	29.7499	-30.6273
24	35	21.3881	10.2184	22.0609	-22.7116
24	36	13.8194	6.60238	14.2541	-14.6745
24	37	0.295738	0.38494	0.201864	-0.197197
24	38	0.242852	0.316102	0.165765	-0.161933
24	39	0.180086	0.234404	0.122922	-0.12008
24	40	0.116358	0.151454	0.079423	-0.077587
25	26	0	0	0	0
25	27	0	0	0	0
25	28	0	0	0	0
25	29	0.6299	0.636844	0.63165	0.680978
25	30	1.50975	2.29322	1.44367	0.427924
25	31	3.86267	3.49105	4.00345	4.25538
25	32	2.21069	2.21397	1.90652	-1.97694
25	33	0.104049	0.042889	0.100591	0.055854
25	34	0.085442	0.035219	0.082602	0.045866
25	35	0.063359	0.026117	0.061254	0.034012
25	36	0.040938	0.016875	0.039577	0.021976
25	37	-3.37658	-3.48989	-3.37037	-3.2053
25	38	-2.77275	-2.8658	-2.76765	-2.6321
25	39	-2.05612	-2.12512	-2.05234	-1.95182
25	40	-1.32851	-1.37309	-1.32607	-1.26112

26	27	0	0	0	0
26	28	0	0	0	0
26	29	0.882355	0.248813	0.924358	1.6996
26	30	2.19732	2.60366	2.16781	1.7268
26	31	6.121	6.48138	6.4281	6.2656
26	32	3.44958	3.70416	3.01814	-3.13632
26	33	-0.186507	-1.10306	-0.196751	0.781767
26	34	-0.153154	-0.905802	-0.161566	0.641965
26	35	-0.113571	-0.671694	-0.119809	0.476047
26	36	-0.073381	-0.433997	-0.077411	0.307585
26	37	-5.43599	-6.1569	-5.45602	-4.47278
26	38	-4.46388	-5.05587	-4.48033	-3.67292
26	39	-3.31017	-3.74916	-3.32237	-2.72364
26	40	-2.13878	-2.42242	-2.14666	-1.75981
27	28	0	0	0	0
27	29	-3.01551	-2.9025	-3.13857	-2.8128
27	30	-4.4742	-4.56275	-4.77815	-4.86235
27	31	2.17285	1.72921	2.31876	2.75302
27	32	-0.016078	-0.296465	-0.272563	-0.203112
27	33	-3.6008	-3.29594	-3.72637	-3.82017
27	34	-2.95687	-2.70653	-3.05999	-3.13702
27	35	-2.19266	-2.00702	-2.26912	-2.32624
27	36	-1.41673	-1.29678	-1.46613	-1.50304
27	37	-1.6486	-0.162341	-1.72581	-3.26918
27	38	-1.35378	-0.13331	-1.41719	-2.68456
27	39	-1.00389	-0.098855	-1.05091	-1.99072
27	40	-0.648639	-0.063873	-0.679017	-1.28625
28	29	-1.1589	-1.42923	-0.906228	0.733525
28	30	-1.52994	-1.63225	-1.21085	1.52192
28	31	2.33298	2.65403	2.30684	-2.35433
28	32	0.748913	0.849346	0.588206	0.716197
28	33	-1.76425	-1.67153	-1.49426	1.49239
28	34	-1.44875	-1.37261	-1.22704	1.22551
28	35	-1.07432	-1.01786	-0.90991	0.908771
28	36	-0.694141	-0.657661	-0.587914	0.587179
28	37	-2.00009	-1.74698	-1.94521	2.17487
28	38	-1.64242	-1.43457	-1.59735	1.78594
28	39	-1.21793	-1.0638	-1.18451	1.32436
28	40	-0.786932	-0.687347	-0.76534	0.855699
29	30	0	0	0	0
29	31	0	0	0	0
29	32	0	0	0	0
29	33	0.240805	0.234426	0.240969	0.261213
29	34	0.197742	0.192504	0.197877	0.214501
29	35	0.146635	0.142751	0.146735	0.159062
29	36	0.094744	0.092234	0.094809	0.102774
29	37	-19.0743	-19.8596	-19.2926	-17.7745
29	38	-15.6633	-16.3081	-15.8425	-14.5959
29	39	-11.615	-12.0932	-11.748	-10.8235
29	40	-7.50475	-7.81373	-7.59064	-6.99335
30	31	0	0	0	0
30	32	0	0	0	0

30	33	0.426929	0.523315	0.42714	0.335557
30	34	0.350582	0.429731	0.350755	0.27555
30	35	0.259973	0.318666	0.260101	0.204333
30	36	0.167975	0.205897	0.168058	0.132024
30	37	-34.8906	-27.5327	-35.834	-39.8478
30	38	-28.6512	-22.6091	-29.4259	-32.7219
30	39	-21.2462	-16.7657	-21.8206	-24.2648
30	40	-13.7277	-10.8327	-14.0988	-15.6781
31	32	0	0	0	0
31	33	0.406311	0.33396	0.422932	0.472674
31	34	0.333651	0.274238	0.3473	0.388147
31	35	0.247418	0.20336	0.257539	0.287829
31	36	0.159862	0.131396	0.166402	0.185973
31	37	39.1671	40.0805	40.7601	36.7978
31	38	32.1629	32.913	33.471	30.2173
31	39	23.8503	24.4065	24.8203	22.4075
31	40	15.4102	15.7696	16.037	14.478
32	33	0.305306	0.281221	0.27772	-0.291323
32	34	0.250709	0.230931	0.228056	-0.239226
32	35	0.185912	0.171246	0.169114	-0.177397
32	36	0.120122	0.110646	0.109269	-0.114621
32	37	5.58747	16.6556	1.98449	-0.413884
32	38	4.58827	13.6771	1.62961	-0.33987
32	39	3.40242	10.1422	1.20843	-0.252029
32	40	2.19838	6.55312	0.780795	-0.162842
33	34	0	0	0	0
33	35	0	0	0	0
33	36	0	0	0	0
33	37	-0.125	-0.191426	-0.124701	-0.023639
33	38	-0.102646	-0.157194	-0.102401	-0.019411
33	39	-0.076117	-0.116566	-0.075935	-0.014394
33	40	-0.049181	-0.075316	-0.049063	-0.009301
34	35	0	0	0	0
34	36	0	0	0	0
34	37	-0.102646	-0.157194	-0.102401	-0.019411
34	38	-0.08429	-0.129083	-0.084089	-0.01594
34	39	-0.062505	-0.095721	-0.062356	-0.01182
34	40	-0.040386	-0.061848	-0.040289	-0.007637
35	36	0	0	0	0
35	37	-0.076117	-0.116566	-0.075935	-0.014394
35	38	-0.062505	-0.095721	-0.062356	-0.01182
35	39	-0.046351	-0.070982	-0.04624	-0.008765
35	40	-0.029948	-0.045863	-0.029877	-0.005663
36	37	-0.049181	-0.075316	-0.049063	-0.009301
36	38	-0.040386	-0.061848	-0.040289	-0.007637
36	39	-0.029948	-0.045863	-0.029877	-0.005663
36	40	-0.01935	-0.029633	-0.019304	-0.003659
37	38	0	0	0	0
37	39	0	0	0	0
37	40	0	0	0	0
38	39	0	0	0	0
38	40	0	0	0	0

39	40	0	0	0	0

Order of Pigments in the RC

1	PD1
2	ChlD1
3	ChlD2
4	PheoD1
5	PheoD2
6	CHlzD1
7	PD2
8	ChlzD2
9	BCR1
10	BCR2

For every Chl a, Pheo a and BCR 4 transitions
Example: The numbers m and n correspond to

m	transition
1	PD1-Qy
2	PD1-Bx
3	PD1-By
4	PD1-Nxy
5	ChlD1-Qy
6	ChlD1-By
…	
40	BCR2 S_0-S_2, Vib_{0-3}